

Quantum dynamics of atoms in number-theory-inspired potentials

D. Cassettari,¹ O. V. Marchukov,² B. Carruthers,¹ H. Kendell,^{3,4} J. Ruhl,⁵ B. De Mitchell Pierre,⁶ C. Zara,⁶ C. A. Weidner,⁴ A. Trombettoni,^{7,8} M. Olshanii,⁵ and G. Mussardo⁸

¹*SUPA School of Physics & Astronomy, University of St. Andrews, North Haugh, St. Andrews KY16 9SS, UK*

²*Technische Universität Darmstadt, Institut für Angewandte Physik, Hochschulstraße 4a, 64289 Darmstadt, Germany*

³*Quantum Engineering Centre for Doctoral Training, University of Bristol, Bristol BS8 1FD, UK*

⁴*Quantum Engineering Technology Laboratories, H. H. Wills Physics Laboratory and Department of Electrical and Electronic Engineering, University of Bristol, Bristol BS8 1FD, UK*

⁵*Department of Physics, University of Massachusetts Boston, Boston Massachusetts 02125, USA*

⁶*Department of Mathematics, University of Massachusetts Boston, Boston Massachusetts 02125, USA*

⁷*Department of Physics, University of Trieste, Strada Costiera 11, I-34151 Trieste, Italy*

⁸*SISSA and INFN, Sezione di Trieste, Via Bonomea 265, I-34136 Trieste, Italy*

(Dated: October 21, 2024)

In this paper we study transitions of atoms between energy levels of several number-theory-inspired atom potentials, under the effect of time-dependent perturbations. First, we simulate in detail the case of a trap whose one-particle spectrum is given by prime numbers. We investigate one-body Rabi oscillations and the excitation lineshape for two resonantly coupled energy levels. We also show that techniques from quantum control are effective in reducing the transition time, compared to the case of a periodic perturbation. Next, we investigate cascades of such transitions. To this end, we pose the following question: can one construct a quantum system where the existence of a continuous resonant cascade is *predicted* on the validity of a particular statement in number theory? We find that a one-body trap with a log-natural spectrum, parametrically driven with a perturbation of a log-natural frequency, provides such a quantum system. Here, powers of a given natural number will form a ladder of equidistant energy levels; absence of gaps in this ladder is an indication of the validity of the number theory statement in question. Ideas for two more resonance cascade experiments are presented as well: they are designed to illustrate the validity of the Diophantus-Brahmagupta-Fibonacci identity (the set of sums of two squares of integers is closed under multiplication) and the validity of the Goldbach conjecture (every even number is a sum of two primes).

I. INTRODUCTION

In recent years, optical trapping of ultracold atoms has advanced to the point that it is now possible to control, with precision, the profile of the trapping potential. This progress has been enabled by “light sculpting” techniques [1] relying on the use of spatial light modulators [2], digital micromirror devices [3, 4], and fast-scanning acousto-optic deflectors [5].

These developments are particularly suited to address in a realistic and tunable setup suggestions and ideas at the interface between quantum physics and number theory [6–8]. To this end, recently, there has been experimental progress in creating prime number potentials for cold atoms [9]. These are trapping potentials whose first N_b eigenenergies are proportional to the first N_b prime numbers. The rationale is that these highly controllable potentials, which can be engineered to have an assigned sequence of numbers as their energy levels, are relevant for a host of theoretical ideas. For instance, they can be used for the implementation of primality tests [6], prime factorization of integers (see [10, 11] and references therein), and for studying statements from number theory such as the Goldbach conjecture, which states that every even natural number greater than two can be written as sum of two prime numbers.

In this paper, we consider one-dimensional trapping potentials in which the position of the individual energy

levels is well-controlled, and we study transitions between energy levels under the effect of time-dependent perturbations. We consider two complementary scenarios:

- In Section II we study transitions in a potential with energy levels proportional to the first N_b prime numbers. Because prime numbers are not regularly spaced, a time-dependent perturbation promotes atoms from the ground state to a given target excited state of the trap, while the population of higher energy states remains negligible. This selective excitation of just one state is useful in view of factorisation algorithms, where it constitutes the initial preparation stage ahead of performing the factorization [11, 12].
- In Sections III and IV we introduce resonance cascades as a paradigm to study statements from number theory. As a test bench, we consider the potential with energy spectrum given by the logarithms of natural numbers. Here we find that because the sequence of natural numbers is closed under multiplication, a perturbation at an appropriate frequency *can* generate a resonance cascade (or ladder), in which many levels are populated.

Finally, in Section V we outline future ideas on how resonance cascades can be used to study the Diophantus-Brahmagupta-Fibonacci identity and the Goldbach conjecture. In the first case, the potential of

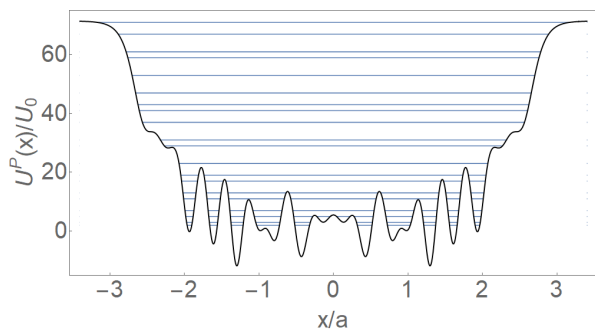


FIG. 1. Prime number potential with 20 energy levels. Here, $a = \hbar/\sqrt{mU_0}$ is the characteristic length scale of the potential (with m the particle mass), and U_0 is the corresponding energy scale.

interest has energy levels given by the logarithm of the sum of two integers squared, whereas the second case is based on the prime number potential investigated in Section II, but in which a cascade is enabled if the potential contains two weakly-interacting particles, each of which has energy equal to a prime number.

II. A RESONANCE IN THE PRIME NUMBER POTENTIAL

A. Periodic perturbations

Fig. 1 shows a prime number potential, defined as the potential entering the single-particle Schrödinger Hamiltonian with eigenvalues given by the first 20 prime numbers:

$$E_n^P = U_0 p_n \quad (1)$$

$$p_1, p_2, p_3, \dots, p_{20} = 2, 3, 5, 7, \dots, 71.$$

This potential has been calculated using the methods of supersymmetric quantum mechanics and has been optically implemented with a spatial light modulator [9].

In this section we simulate the transfer between bound states of this prime number potential by applying time-dependent perturbations of the form:

$$V(x, t) = f(x) \cos(\omega t)$$

where we examine two cases for $f(x)$ (see Fig. 2): $f_{odd}(x) = \beta(x/a)$ and $f_{even}(x) = \beta(x/a)^2$, which induce transitions between states of opposite parity and of same parity respectively. Specifically, using $f_{odd}(x)$ enables the transfer between the ground state $|0\rangle$ and the first-excited state $|1\rangle$, while using $f_{even}(x)$ enables the transfer between state $|0\rangle$ and the second-excited state $|2\rangle$. In both cases, the perturbation is close to resonance with the transition ($\omega = U_0/\hbar$ for first excited and $\omega = 3U_0/\hbar$ for the second excited), and the anharmonicity of the potential ensures that the population of higher states remains

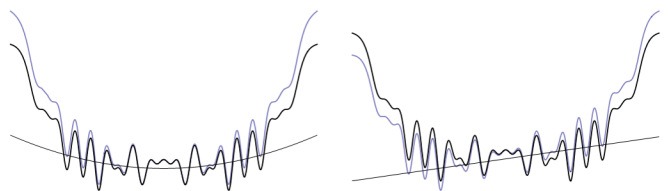


FIG. 2. Even and odd perturbations. $\beta = 2$ for the even case and $\beta = 4$ for the odd case. These β values are significantly larger than those used in the simulations to better visualise the effect of the perturbations on the potential.

small, so that we have essentially a two-level system. Experimentally, these perturbations can be realized with additional optical fields. Fig. 3 shows Rabi oscillations between $|0\rangle$ and $|1\rangle$ (a), and between $|0\rangle$ and the $|2\rangle$ (b), obtained by numerical integration of the time-dependent Schrödinger equation. The Rabi frequency Ω_R is given by the matrix element of the perturbation between the ground state and the desired excited state [13]. The β values are chosen according to the following criterion: a larger β would lead to a higher Rabi frequency and a faster transfer to the desired excited state, which is experimentally advantageous, however this would come at the price of reduced efficiency of the transfer to the desired excited state, because a larger β would increase the population of higher states. In this respect, Fig. 3 shows the fastest possible transfer while achieving a good population of $> 98\%$ of the desired excited state.

In addition to the Rabi oscillations, the time evolution also displays fast ripples at frequency 2ω . These are due to the fact that the rotating wave approximation is not perfectly satisfied for the perturbation strengths we are using.

To further characterize the system, we study the effect of off-resonant perturbations. For a two-level system in the rotating wave approximation, the maximum population of the excited state is:

$$P_{ex,max} = \frac{\Omega_R^2}{\Omega_R^2 + \delta^2} \quad (2)$$

where δ is the detuning from resonance [13]. The maximum population is 1 for resonant perturbation ($\delta = 0$), and displays a Lorentzian lineshape for finite detunings with $\text{FWHM} = 2\Omega_R$. These Lorentzian lineshapes are found numerically in our system for both the odd and the even transition, as shown in Fig. 4. The good agreement between the numerical data and Eq. 2 (with the value of Ω_R calculated from the relevant matrix element of the perturbation) shows that our system behaves as a two-level system to a good approximation. We note that for larger values of β , the center of the transition slightly shifts to the right. We attribute this to the Bloch-Siegert effect [14], which occurs beyond the rotating wave approximation. Similarly, the deviation of the numerical data from the Lorentzian, visible at positive detunings,

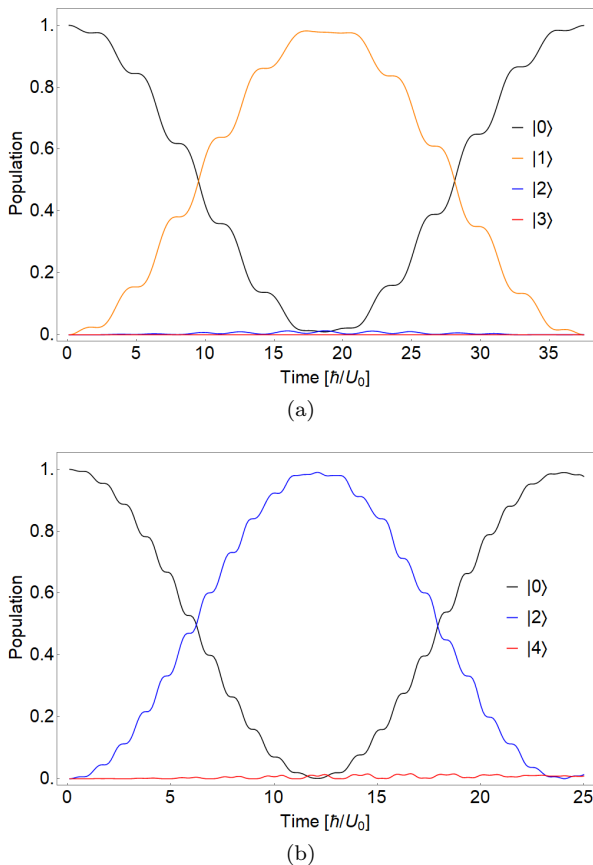


FIG. 3. (a) Odd transition between the ground state and first excited state with $\beta = 0.25$. (b) Even transition between the ground state and second excited state with $\beta = 0.5$. This strength leads to a small but visible population of the fourth excited state (the next transition of even parity).

is also likely due to the rotating wave approximation not being well satisfied.

In an experimental implementation with ultracold atoms (for instance rubidium), the typical resonance frequencies will be ~ 1 Hz and typical transfer times to the excited state will be of the order of 10 s. These slow timescales are due to the fact that the characteristic length scale of the potential a needs to be well above the optical resolution of the optical system that produces the potential. This constraint on a puts an upper limit on U_0 via $a = \hbar/\sqrt{mU_0}$, and consequently a lower limit on the time unit \hbar/U_0 [9].

Experimentally, it will be desirable to speed up the time evolution. But this cannot be achieved by increasing the strength β of the perturbation without increasing the population of higher states as well, therefore reducing the efficiency of the transfer to the desired state. Hence in the following section, we speed up state transfer through optimal control methods.

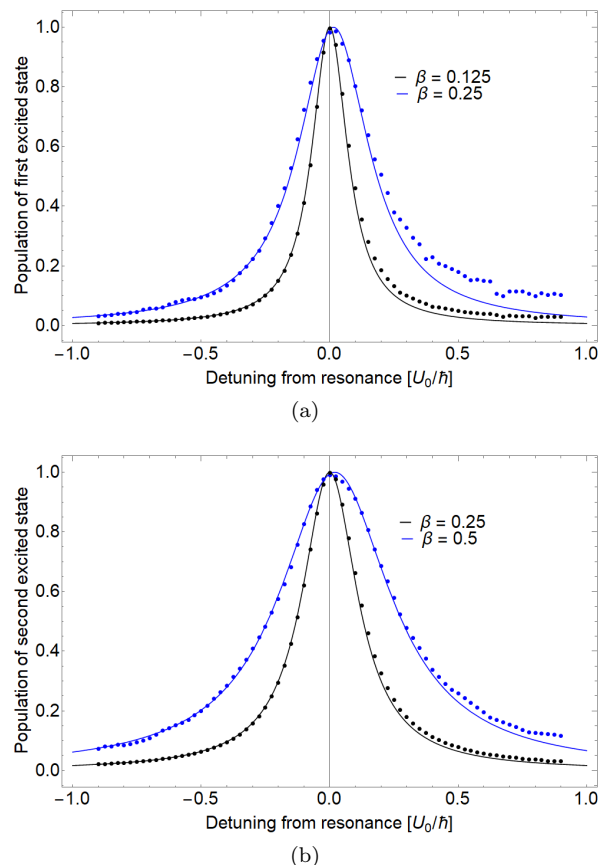


FIG. 4. (a) Lineshape of the odd transition for $\beta=0.125$ and $\beta=0.25$. (b) Lineshape of the even transition for $\beta=0.25$ and $\beta=0.5$. All sets of numerical data are displayed alongside the Lorentzian Eq. (2) with their respective value of Ω_R . We note that for the same value $\beta=0.25$, the width of the odd transition is larger than the width of the even transition. This is due to the different couplings in these two cases: $\langle 0|x|1\rangle = 0.68$ and $\langle 0|x^2|2\rangle = 0.52$.

B. Quantum control

In this section, we explore two state transfer protocols optimized using the GRAPE algorithm [15] and the QEngine C++ library [16]:

- $\beta(x/a)^2$ modulation for $|0\rangle \rightarrow |2\rangle$ transfer,
- $\beta(x/a)$ modulation for $|0\rangle \rightarrow |1\rangle$ and $|0\rangle \rightarrow |3\rangle$ transfer.

For each case, we implemented a control of the form $\beta b(t)(x/a)^n$ with $n = 1, 2$ for the linear and quadratic cases, respectively. The control $b(t)$ was optimized for a given static value of β , and $-1 \leq b(t) \leq 1\forall t$.

These protocols provide a benchmark that serves to compare optimal control results with resonant driving results, as well as demonstrating an interesting state preparation proof-of-principle that can be useful for, e.g., the resonant cascade protocols described in later sections

Transfer Time (\hbar/U_0)	$ 1\rangle$	$ 2\rangle$	$ 3\rangle$
$\beta = 0.5, n = 2$	-	9.5	-
$\beta = 1, n = 2$	-	5.0	-
$\beta = 2, n = 2$	-	3.0	-
$\beta = 10, n = 2$	-	2.0	-
$\beta = 0.5, n = 1$	7.5	-	$\gg 12.0$
$\beta = 1, n = 1$	5.5	-	9.0
$\beta = 2, n = 1$	4.0	-	7.0

TABLE I. Optimized transfer times ($\mathcal{F} > 0.99$) from the ground state for a variety of protocols. Note that controls with final time shown as $\gg 12\hbar/U_0$ have not been optimized for longer times due to computer cluster limitations.

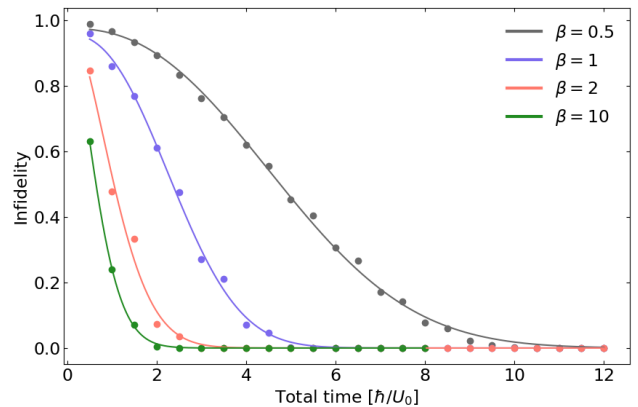
of this manuscript. For the optimization, the initial state is the ground state of the prime number potential, and we use regularization [17, 18] to limit the bandwidth of the control in order to preserve experimental viability.

Using the unit scalings provided, the best results are tabulated in Table I, and plots of the fidelity vs. control time for $\beta(x/a)^2$ and $\beta(x/a)$ are shown in Fig. 5. These show the minimum time required for a control to reach 0.99 fidelity, where fidelity is defined as $\mathcal{F} = |\langle \psi_{\text{des}} | \psi_{\text{opt}} \rangle|^2$, with $|\psi_{\text{des}}\rangle$ corresponding to the either $|1\rangle$, $|2\rangle$, or $|3\rangle$ and $|\psi_{\text{opt}}\rangle$ the final state after optimization. The infidelity is $\mathcal{I} = 1 - \mathcal{F}$. The optimal controls (i.e., those found at the minimum time where $\mathcal{F} > 0.99$) are plotted in Fig. 6 for $\beta = 0.5$.

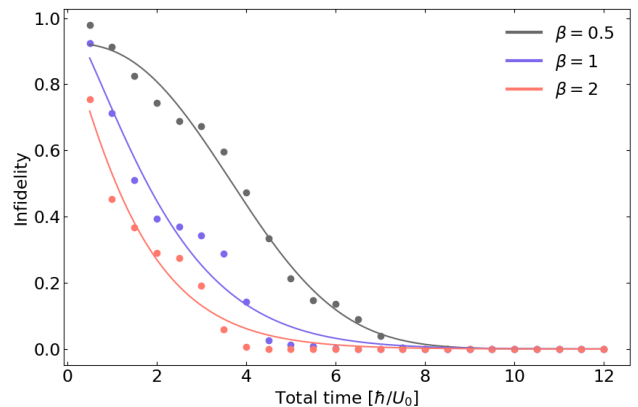
The results in Table I show that quantum control enables the transfer to the desired excited state with fidelities comparable to the case of the periodic perturbations, but with reduced transfer times. Differently from the case of periodic perturbation, with quantum control it is possible to increase β , hence reducing significantly the transfer time, while keeping the population of higher levels negligible. All the transfer times reported on Table I correspond to experimental times of 5 s or less.

III. RESONANCE CASCADES

In this section we introduce the idea of using *resonance cascades* to study statements from number theory: given a number-theoretical statement, we will first recast the statement or some of its corollaries as an assertion of an existence of an *uninterrupted* arithmetic progression as a subsequence of a larger sequence of numbers (the *principal sequence*). The latter sequence will constitute the energy spectrum of a quantum system. The step in the arithmetic subsequence in question will correspond to the frequency of a time-dependent perturbation. If the arithmetic progression is fully contained in the principal sequence, the corresponding quantum system will be able to travel along the energy axis efficiently, exclusively via *resonant* transitions. The following three examples are considered in this paper:



(a) $\beta(x/a)^2$



(b) $\beta(x/a)$

FIG. 5. Infidelity vs. time curves for (a) $|0\rangle \rightarrow |2\rangle$ transfer with $\beta(x/a)^2$ modulation and (b) $|0\rangle \rightarrow |1\rangle$ transfer with $\beta(x/a)$ modulation. The strength of the β value are labelled in the plot legends. The individual data points are the best results of 2000 optimizations, and the line is a guide to the eye.

- (I) The number-theoretic statement: *The sequence of natural numbers is closed under multiplication.*

Corollary to be studied: *Given a natural number \tilde{n} , any power of it, $(\tilde{n})^m$, will be present in the sequence of natural numbers.*

The principal sequence of numbers: $\ln(n)$ with $n = 1, 2, 3, \dots$

The arithmetic progression: $m \ln(\tilde{n})$ with $m = 0, 1, 2, 3, \dots$, with \tilde{n} being a natural number.

The corresponding quantum system: one particle in a trap whose energy spectrum is proportional to the logarithms of natural numbers, $E_n = U_0 \ln(n)$, $n = 1, 2, 3, \dots$. The excitation frequency will be given by $\hbar\Omega = U_0 \ln \tilde{n}$.

- (II) The number-theoretic statement: *The sequence of sums of two squares on integers is closed*

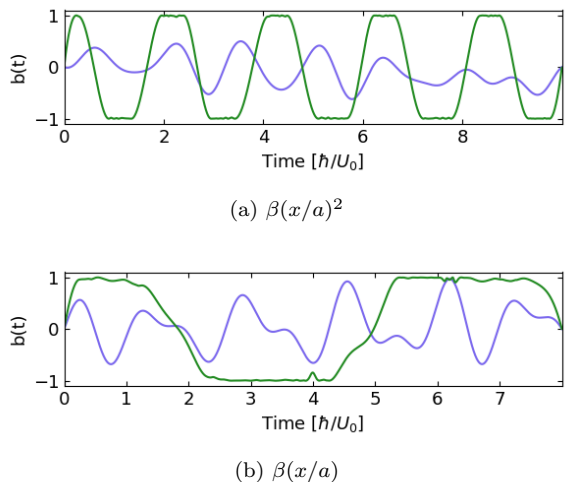


FIG. 6. Optimal controls $b(t)$ for (a) $\beta(x/a)^2, |0\rangle \rightarrow |2\rangle$ transfer and (b) $\beta(x/a), |0\rangle \rightarrow |1\rangle$ transfer. Here $\beta = 0.5$. The blue (green) line denotes the initial (optimized) control.

under multiplication (Diophantus-Brahmagupta-Fibonacci identity [19] (Lemma 1, p. 142)).

Corollary to be studied: *Given a sum of two squares \tilde{s} , any power of it, $(\tilde{s})^m$, will be present in the sequence of sums of two squares.*

The principal sequence of numbers: $\ln(s_n)$ with $s_1 = 0^2 + 1^2 = 1$, $s_2 = 1^2 + 1^2 = 2$, $s_3 = 0^2 + 2^2 = 4$, $s_4 = 1^2 + 2^2 = 5$, $s_5 = 2^2 + 2^2 = 9$, ... [20]

The arithmetic progression: $m \ln(\tilde{s})$ with $m = 0, 1, 2, 3, \dots$, and \tilde{s} being a nonzero sum of two squares.

The corresponding quantum system: one particle in a trap whose energy spectrum is proportional to the logarithms of sums of two squares numbers, $E_n = U_0 \ln(s)$, $n = 1, 2, 3, \dots$. Excitation frequency will be given by $\hbar\Omega = U_0 \ln \tilde{s}$.

- (III) The number-theoretic statement: *Any even number greater than 2 is a sum of two primes* (Goldbach conjecture [19] (p. 147)).

Corollary to be studied: Any even number greater than 4 is a sum of two primes greater than 2.

The principal sequence of numbers, with degeneracies: $w_{n,l}$ with $w_1 = 3 + 3 = 6$, $w_2 = 3 + 5 = 8$, $w_{3,1} = 5 + 5 = 10$, $w_{3,2} = 3 + 7 = 10$, $w_4 = 5 + 7 = 12$, ...

The arithmetic progression: $m \times 2$ with $m = 3, 4, 5, \dots$

The corresponding quantum system: two interacting particles in a trap whose one-body energy spectrum, $E_n^{(1)} = U_0 p_n$, $n = 2, 3, 4, 5, \dots$ is proportional to the prime numbers greater than 2: i.e. 3, 5, 7, 11 ... Excitation frequency will be given by $\hbar\Omega = U_0 \times 2$.

Example (I), which is to be regarded as a proof-of-principle, is studied in depth in Section IV. For examples (II) and (III), we only outline ideas for future experiments in Section V.

IV. RESONANCE CASCADE PREDICATED ON CLOSENESS OF THE NATURAL SET UNDER MULTIPLICATION

A. The set-up

Consider a one-body potential $U^L(x)$ whose lowest N_b bound state energies are given by

$$\begin{aligned} E_n^L &= U_0 \ln n \\ n &= 1, 2, 3, \dots, N_b \end{aligned} \quad (3)$$

Figure 7(a) shows this potential for $N_b = 30$. Similarly to the prime number potential of Section II, this potential is designed using supersymmetric methods [9]. As N_b increases, the potential converges to a smooth classical limit. This classical counterpart can be extracted using procedures developed in classical mechanics (see §12 in [21]). There is a variety of classical potentials that can approximate our quantum potential: one of them is a logarithmic potential:

$$U_{\text{cl.}}^L(x) = U_0 \ln \left(\sqrt{\frac{2x}{\pi a}} \right), \quad (4)$$

where $a \equiv \hbar/\sqrt{mU_0}$ (see Appendix A 1).

Note that the existence of the classical limit of an artificially constructed potential with an *a priori* prescribed spectrum is not guaranteed. Figure 7(b) shows a potential whose first $N_b = 30$ energy levels are proportional to the first 30 integers that are equal to the sum of two squares. We see that as N_b increases, this potential retains its substantially quantum nature: the small potential wells can be shown to contain only one or two eigenstates.

B. Protocol

Let us choose a natural number of interest, \tilde{n} and its initial power, m_0 . Our goal is to propose an effect that would be predicated on the presence of all powers of \tilde{n} (up to a practical upper limit) in the set of natural numbers.

To this end, consider a single atom (or an ensemble of noninteracting atoms) in an excited state $|n = \tilde{n}^{m_0}\rangle$, with $\tilde{n}^{m_0} < N_b$. Next, we apply a parametric perturbation

$$V(x, t) = \epsilon \cos(\Omega t) U^L(x), \quad (5)$$

where

$$\Omega = \frac{1}{\hbar} U_0 \ln(\tilde{n}), \quad (6)$$

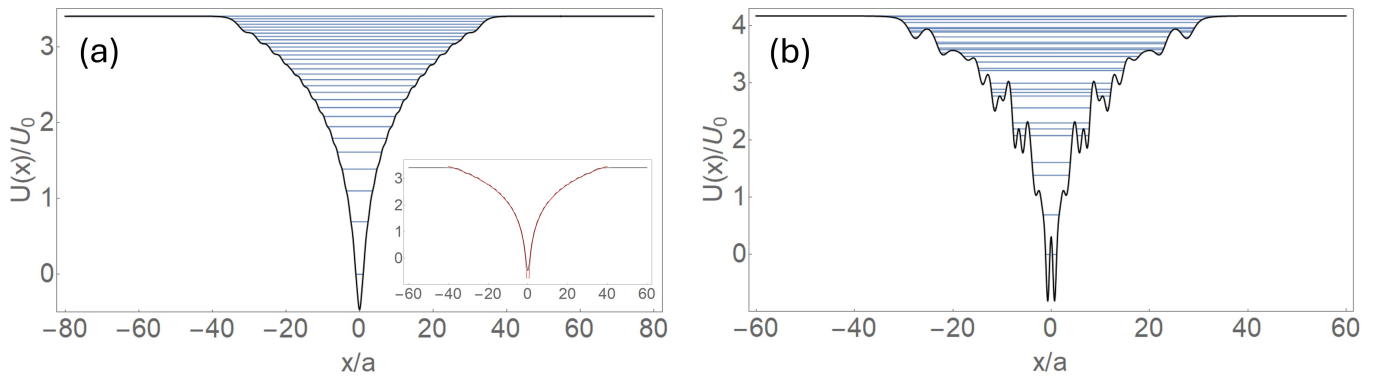


FIG. 7. **Two potentials with a prescribed spectrum.** (a) A potential whose lowest 30 energy levels are proportional to the logarithms of the first 30 natural numbers. Insert: This potential is compared to its classical counterpart (4). (b) A potential whose lowest 30 energy levels are proportional to the logarithms of sums of two squares.

with $\epsilon \ll 1$. The full Hamiltonian becomes

$$\hat{H}^L = \frac{\hat{p}^2}{2m} + (1 + \epsilon \cos(\Omega t)) U^L(x).$$

This perturbation will induce a *resonance cascade*, i.e., a cascade of resonant transitions between states:

$$|n = 1\rangle \overset{\Omega}{\leftrightarrow} |n = \tilde{n}\rangle \overset{\Omega}{\leftrightarrow} |n = \tilde{n}^2\rangle \overset{\Omega}{\leftrightarrow} \dots \overset{\Omega}{\leftrightarrow} |n = \tilde{n}^m\rangle \overset{\Omega}{\leftrightarrow} \dots \overset{\Omega}{\leftrightarrow} |n = \tilde{n}^{m_0}\rangle \overset{\Omega}{\leftrightarrow} |n = \tilde{n}^{m_0+1}\rangle \overset{\Omega}{\leftrightarrow} \dots, \quad (7)$$

which will cause the population to spread over energy levels in a resonant manner. An ability of our system to reach the $|n = 1\rangle$ would serve as a “proof” that each of the numbers $1, \tilde{n}, \tilde{n}^2, \dots, \tilde{n}^{m_0}$ belongs to the set of naturals.

Our first numerical experiment featured the following set of parameters:

$$\begin{aligned} N_b &= 120 \\ \tilde{n} &= 3 \\ m_0 &= 3 \text{ (i.e. initial state was } |n = 27\rangle \text{)} \\ \epsilon &= 0.3. \end{aligned} \quad (8)$$

Fig. 8(a) shows our results. While the members of the cascade (7) clearly dominated the population (see the left insert), the population was localized in the vicinity of $m = 3$ and $m = 2$.

In order to understand the origin of this localization we analyzed the behavior of the off-diagonal matrix elements of our perturbation, $\langle n' | U^L | n \rangle$ (Fig. 9(a)). We found an inverse-linear dependence on the magnitude of the quantum number difference, $|n' - n|$. This assertion was well supported by the large- $|n' - n|$ asymptotics of the semiclassical approximation for the matrix elements

(Appendix A 4 and formula (A12) there) that gives

$$\langle n' | U^L | n \rangle \overset{|n' - n| \gg 1}{\approx} \begin{cases} (-1)^{\frac{n' - n}{2} - 1} \frac{U_0}{|n' - n|} & \text{for } n' - n = \text{even} \\ 0 & \text{for } n' - n = \text{odd} \end{cases}.$$

Numerically, we found a dependence

$$|\langle n' | U^L | n \rangle| \overset{|n' - n| \gg 1}{\approx} A \frac{U_0}{|n' - n|},$$

with $A = 0.80$ for $n = 60$ ((A13)), while our analytic result (A12) predicts $A = 1$.

In terms of the cascade states, Eq. (7), an inverse linear dependence of the transition matrix elements on $|n' - n|$ leads to an exponential decay of the hopping constant within the cascade:

$$|\langle n' = \tilde{n}^{m+1} | U^L | n = \tilde{n}^m \rangle| \sim U_0 e^{-\gamma m}$$

with $\gamma = \ln(\tilde{n})$ (see the caption of Fig. 9 and Appendix B 6 for a more precise formulation of this connection). Under a rotating wave approximation, the system becomes a tight-binding model with the hopping coefficients J_m (between the m -th and $m + 1$ -st sites) that

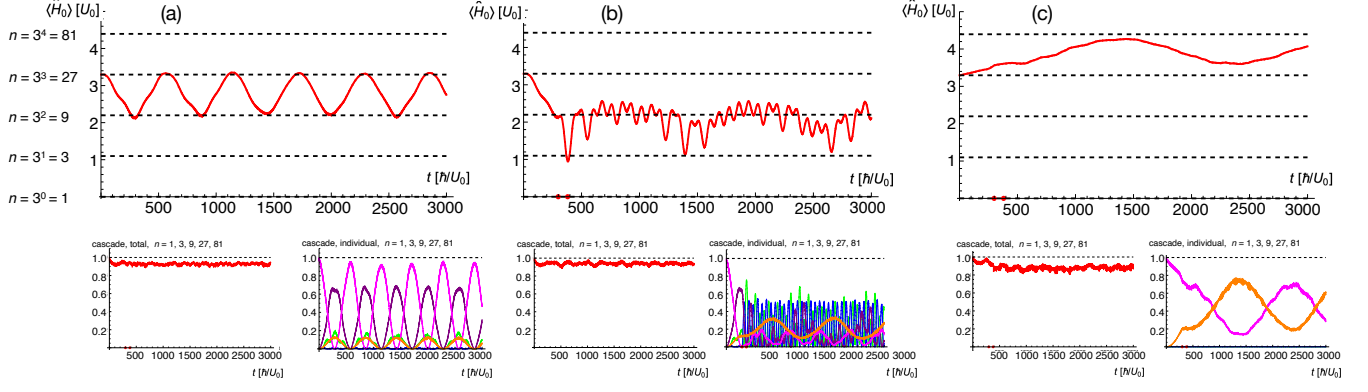


FIG. 8. **A numerical experiment aimed to verify if all powers of 3 are present in the set of natural numbers.** A single atom, initially placed in the $|n = 27\rangle$ state of the potential $U(x)$ whose spectrum, (3), is given by $E_n = U_0 \ln(n)$ ($n = 1, 2, 3, \dots, 120$) is subjected to a periodic perturbation of the form $V(x, t) = \epsilon U(x) \cos(\Omega t)$, with $\epsilon = 0.3$, and $\Omega = \frac{1}{\hbar} U_0 \times \ln(\tilde{n})$, where $\tilde{n} = 3$. In all three subfigures, the left inset shows the total population of the resonance cascade states, $|n = 1\rangle, |n = 3\rangle, |n = 9\rangle, |n = 27\rangle, |n = 81\rangle$; in all three cases, the cascade comprises no less than 80% of the total population. The right insets show populations of the individual members of the cascade: (green) $|n = 1\rangle$, (blue) $|n = 3\rangle$, (purple) $|n = 9\rangle$, (magenta) $|n = 27\rangle$, (orange) $|n = 81\rangle$. (a) Mobility is impeded due to “dark state” localization (Subsec. B 1). Indeed, the right inset shows that the time evolution is close to Rabi oscillations between $|n = 27\rangle$ and $|n = 9\rangle$. (b) In this numerical experiment, we introduce four “windows of silence” of a duration $\Delta t = \frac{\pi}{\Omega}$, at $t = \{298.83, 380.31\} \times \hbar/U_0$ (red dots on the abscissa), during which the perturbation is stopped and then restarted after a quarter of of the perturbation period, in the phase it had just before the window. The windows are designed to break the “dark states” and in doing so, promote mobility along the energy axis. The level population indeed starts moving down in energy, while remaining within the set of resonantly coupled energy levels $U_0 \times \log(n = 3^m)$. Right insert shows that all five states comprising the resonance cascade become substantially populated. (c) A gedanken experiment where $n = 9$ is excluded from the set of natural numbers. At a technical level, we create a potential with a spectrum $E_n = U_0 \ln(n)$ ($n = 1, 2, 3, \dots, 8, 11, 12, \dots, 120$) where the $n = 9$ energy level is excluded. We also exclude the $n = 10$ level in order to preserve the relative parity of the remaining eigenstates. Such an exclusion can be seen to impede the mobility along the energy axis. In this experiment, we apply the same “silence windows” as in the in the (a) computation. Right insert shows that the time evolution is close to Rabi oscillations between $|n = 27\rangle$ and $|n = 81\rangle$.

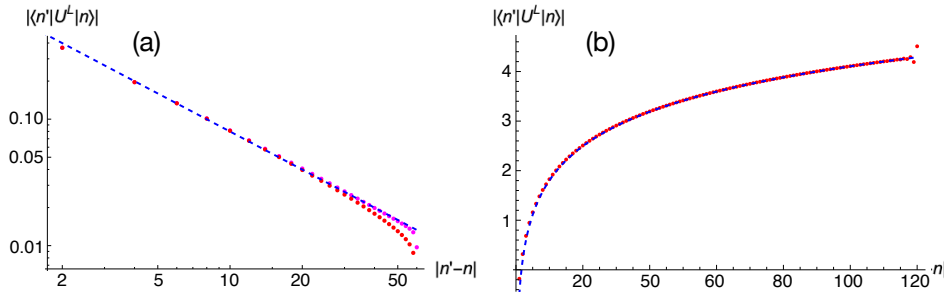


FIG. 9. **Semiclassical approximation for the matrix elements of the perturbation (represented, in the case of a parametric excitation, by the potential energy) compared to the numerical results.** (a) Absolute value of the off-diagonal matrix elements of the potential energy, $\langle n' | U^L | n = 60 \rangle$, as a function of the absolute value of the index difference, $n' - n$. Only even values of $n' - n$ are represented, since the odd values vanish due to the parity selection rule. The magenta dots represent the numerical results for $n' > n$, while the red dots correspond to $n' < n$. The $\ln(n)$ -spectrum potential used had $N_b = 120$ bound states. The blue dashed line is the semiclassical prediction $|\langle n' | U^L | n \rangle| \approx A U_0 / |n' - n|$ (see Eq. (A13)) with the value of the fit parameter $A = 0.80$ representing the best fit for the data with $4 \geq |n' - n| \leq 30$. The coefficient J_0 and the decay constant γ in the exponential lattice model of Appendix B (Eq. (B1)) will be then given by $J_0 = \epsilon \frac{A}{(\tilde{n}-1)}$ and $\gamma = \ln(\tilde{n})$ respectively. (b) Numerically computed diagonal matrix elements of the potential energy, $\langle n | U^L | n \rangle$, in comparison with the virial formula (A14); no fit parameters were used.

exponentially decay as a function of m :

$$\hat{H}_{\text{EL}} = -J_0 \sum_{m=-\infty}^{+\infty} e^{-\gamma m} (|m+1\rangle\langle m| + |m\rangle\langle m+1|) \quad (9)$$

(see, also (B1)). In Appendix B we studied the resulting lattice in detail. Indeed, we found a localization for any eigenstate energy E .

While a localization in the “classically forbidden” region of high m where $|E| \gg J_m$ was expected, a localization in the direction of lower m , where $|E| \ll J_m$ required an explanation. We found that in that area, the eigenstate wavefunction becomes a member of the kernel of the Hamiltonian, i.e. a state such that the action of the Hamiltonian on it is null (see Subsection B1). The structure of the such a “dark state” wavefunction ([22, 23]) is as follows (cf. Fig. 14). The population of the odd sites is zero. The amplitudes of the even sites form a coherent superposition to ensure that the population of the odd sites remains at zero, when the Hamiltonian in Eq. (9) acts on such a superposition. On the other hand, since the even sites have unpopulated neighbors, the action of the Hamiltonian Eq. (9) on such a state is zero. (Interestingly, we found that any boundary condition at low m would instantly favor the sites of one parity over another; in the convention used, it is indeed always the odd sites that remain unpopulated in the low m tail of the eigenstates.) Finally, in Subsection B1, we show that the coherence a “dark state” relies on leads to an exponential decay of the population in space.

To promote mobility along the energy axis, we considered the following amendment to our protocol. Whenever localization occurs, we stop the excitation for a quarter of its period (i.e. for a time interval $\Delta t = \frac{\pi}{2\Omega}$) and then restart the excitation in the phase it was in the beginning of the “silence window”. It is easy to see that the free evolution during Δt flips the relative sign of the neighboring even sites, thus breaking the coherence of the “dark state” tail. Fig. 8(b) shows that this is indeed a valid strategy. With only four “silence windows” we were able to transport the population towards the ground state, while traveling exclusively through the resonance ladder. Thus this experiment “demonstrates” that powers of 3 (lower than or equal to 3) are present in the set of natural numbers.

Finally, we simulate a fictitious universe where $3^2 = 9$ is not a natural number. In Fig. 8(c), we consider a potential with a spectrum similar to the simulation (b) but with $n = 9$ level excluded (along with $n = 10$ level, to preserve the relative parity of the remaining eigenstates). The downward energy transfer stops there affirming the ability of our procedure to notice holes in energy-equidistant ladders of the quantum eigenstates [24].

In an experimental implementation, the dynamics shown in Fig. 8 will be observable in less than 10 s, i.e. on a similar timescale to the dynamics presented in

Section II, even though the time axis in Fig. 8 extends to larger values than the time axis in the figures of Section II. The reason is as follows: the value of the energy scale U_0 is larger for the logarithmic potential than for the prime number potential. This is due to the “cusp”-like shape of logarithmic potential, which is narrower than the “flat” shape of the prime number potential, leading to a larger spacing between the energy levels. This larger energy scale U_0 gives a smaller time unit \hbar/U_0 . Hence, the physical time span of Fig. 8 ends up being comparable to the time spans of Section II.

C. Discussion and further work

In future, we would like to address two aspects of the protocol presented above:

1. In this study we have used a parametric perturbation. We had previously considered power-law perturbations, such as the quadratic perturbation used in Section II, but we found that in this case the transition matrix elements change more rapidly over the cascade, compared to the $|n' - n|^{-1}$ dependence for the case of the parametric perturbation. Hence power-law perturbations appear to be less favourable for cascades. However other choices of perturbation could lead to a better behaviour of the matrix elements, with the ideal perturbation being one that gives approximately constant matrix elements over the cascade. This will be an area of further investigation.
2. In the current scheme, we position the “windows of silence” ad hoc. Finding the optimal number and timing of the windows required numerical experimentation. In the future, we would like to find a recipe that will be able to suggest the optimal sequence of the “windows of silence” without a need for a prior numerical or empirical experiments.

V. FUTURE EXPERIMENTS WITH RESONANCE CASCADES

A. Resonance cascade predicated on the validity of the Diophantus-Brahmagupta-Fibonacci identity

The set of natural numbers is not the only set of integers that is closed under multiplication. As follows from the Diophantus-Brahmagupta-Fibonacci identity [19] (Lemma 1, p. 142), the set of integers that are equal to the sums of two squares (see (10)) also has this property.[25] [26] An example of a potential whose spectrum is proportional to the sequence (10) is shown in Fig. 7(b).

Similarly to the case of a $\ln(n)$ -spectrum potential

(Fig.7(a)), the $\ln(s)$ -spectrum potential,

$$\begin{aligned} E_n^{L2} &= U_0 \ln s_n \\ s_1, s_2, s_3, s_4, \dots &= \\ &= (0^2 + 1^2), (1^2 + 1^2), (0^2 + 2^2), (1^2 + 2^2), \dots \\ n &= 1, 2, 3, \dots, N_b \end{aligned} \quad (10)$$

where the integers s are each the sum of two squares, will support unbounded cascades of resonant transitions. For that to happen, the frequency of the perturbation must have the form

$$\Omega = \frac{1}{\hbar} U_0 \ln s_{\bar{n}},$$

where $s_{\bar{n}}$ is itself a sum of two squares.

Note that for technical reasons, we exclude $0^2 + 0^2 = 0$ from the set Eq. (10).

B. Resonance cascade predicated on the validity of the Goldbach conjecture

Unlike the $\ln(n)$ -spectrum potential considered above, a one-body potential whose spectrum is given by the prime numbers already exists [9] and has been examined in Section II. As a slight modification, here we will exclude 2 from the set of primes. Then, the potential we are interested in will produce the following one-body spectrum:

$$\begin{aligned} E_n^P &= U_0 p_n \\ p_1, p_2, p_3, p_4, \dots &= 3, 5, 7, 11, \dots, \\ n &= 1, 2, 3, \dots, N_b \end{aligned} \quad (11)$$

Consider two bosonic atoms in a p -spectrum trap (see Fig. 10). For the moment, let us set interactions to zero. Let us apply a weak *one-body* periodic perturbation $\hat{V} \cos(\Omega t)$ of frequency

$$\Omega = \frac{1}{\hbar} U_0 \times 2.$$

Let us start from the ground state, $|3, 3\rangle$, and explore the possibility of traveling infinitely high in energy, via resonant transitions *only*.

Consider two energy-consecutive two-body eigenstates $|p_1, p_2\rangle$ and $|p'_1, p'_2\rangle$, with

$$\begin{aligned} w &= p_1 + p_2 \\ w' &= p'_1 + p'_2 \\ p_2 &\geq p_1 \\ p'_2 &\geq p'_1 \\ w' &= w + 2. \end{aligned}$$

(Their energies are given by

$$\begin{aligned} E &= \hbar U_0 w \\ \text{and} \\ E' &= \hbar U_0 w' = E + U_0 \times 2 \end{aligned}$$

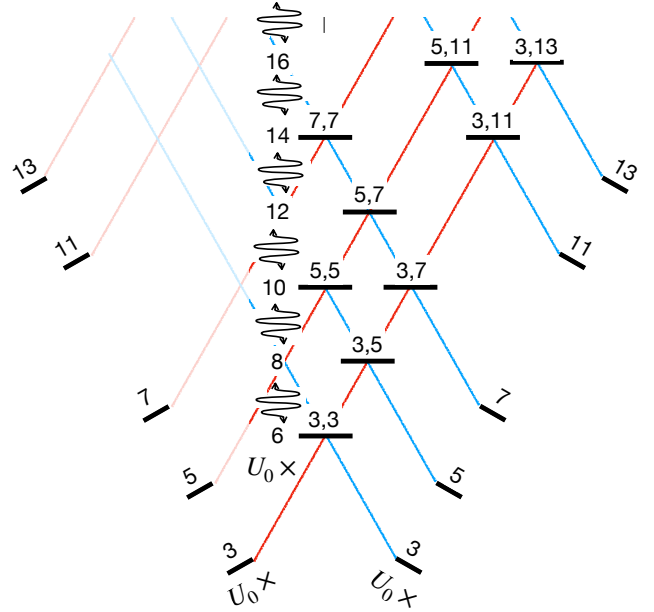


FIG. 10. **Energy spectrum of two weakly interacting bosons in a p -spectrum potential.** The energy levels, $E = U_0 \times 4, 6, 8, \dots$, are formed by sums of two prime numbers, p_1 and $p_2 \geq p_1$. In the text, we suggest applying a weak periodic one-body resonant perturbation of frequency $(U_0/\hbar) \times 2$. Up to the level $E = U_0 \times 38$, the one-body transitions alone ensure the resonant upward mobility of the system, thanks to a proliferation of twin prime pairs. The gap between $E = U_0 \times 38$ and $E' = U_0 \times 40$, inaccessible for one-body processes, can be overcome by weakly mixing the original eigenstates using a two-body interaction. Finally, a complete upward mobility of the level population is predicated on the validity of Goldbach's conjecture.

respectively.) If at least one of the primes p_1, p_2 participating the Goldbach decomposition of the even w is a lower member of a twin prime pair (a “lower twi” from now on) [27], then $|p_1, p_2\rangle$ and $|p'_1, p'_2\rangle$ will be resonantly coupled with a nonzero matrix element. That is, the one-body nature of the perturbation imposes the following selection rule for the transition

$$w \rightarrow w' = w + 2 :$$

$$\begin{aligned} p'_1 &= p_1 + 2 \text{ and } p'_2 = p_2 \\ \text{or} \\ p'_2 &= p_1 + 2 \text{ and } p'_1 = p_2 \\ \text{or} \\ p'_1 &= p_2 + 2 \text{ and } p'_2 = p_1 \\ \text{or} \\ p'_2 &= p_2 + 2 \text{ and } p'_1 = p_1 \end{aligned} \quad (12)$$

For the allowed transitions, the transition matrix element

can be estimated as

$$\langle p'_1, p'_2 | \hat{V} \otimes \hat{I} + \hat{I} \otimes \hat{V} | p_1, p_2 \rangle \sim \langle p' | \hat{V} | p \rangle ,$$

where $\langle p' | \hat{V} | p \rangle$ is a typical one-body matrix element of \hat{V} .

$$\langle p'_1, p'_2 | \hat{V} \otimes \hat{I} + \hat{I} \otimes \hat{V} | p_1, p_2 \rangle \sim \frac{\langle p' | \hat{V} | p \rangle \langle p'_I, p'_{II} | \hat{V}^{(2)} | p_I, p_{II} \rangle}{U_0} ,$$

where $\langle p'_I, p'_{II} | \hat{V}^{(2)} | p_I, p_{II} \rangle$ is a typical two-body matrix element of $\hat{V}^{(2)}$.

In Appendix C, we prove that the number of the two-body energy levels that require two-body interactions to be resonantly coupled with the next level above (equivalently, that there exists an infinite number of even numbers whose Goldbach decomposition does not involve lower twin primes) is infinite.

Finally, it may so happen that for a given two-body energy level E , the required level above, of an energy $E + U_0 \times 2$, has no eigenstates. In the number theory language, this would mean that the even number w' can not be represented as a sum of two primes. However, that would contradict Goldbach's conjecture, which states that every even number greater than 2 is the sum of two prime numbers. (In this work, we will be using an equivalent formulation: every even number greater than 4 is a sum of two primes each greater than 2.)

If we assume that Goldbach's conjecture is valid, we can expect that starting from the ground state of our system, we can reach any of its excited states via resonant transitions alone.

VI. CONCLUSIONS

In this paper we have examined different potentials, namely prime number potentials and logarithmic potentials, which are relevant for applications of quantum physics to number theory. First, we have studied the case in which the system behaves as a two-level system due to the unequal spacing between the energy levels. We have shown that, starting from the ground state, we can prepare an individual excited state with high fidelity. Transfer time can be reduced with quantum control techniques.

The first one-body-forbidden transition occurs at

$$w = 38 = 7 + 31 = 19 + 19$$

$$w' = 40 = 3 + 37 = 11 + 29 = 17 + 23 ,$$

and it is not known yet whether the number of such transitions is infinite or finite. To break the selection rules (12), one will need to consider adding a weak two-body interaction potential $\hat{V}^{(2)}$. In this case, the previously forbidden transition $|p_1, p_2\rangle \rightarrow |p'_1, p'_2\rangle$ becomes weakly allowed. In the first order of the perturbation theory with respect to $\hat{V}^{(2)}$, the transition matrix has the following estimate:

Next, we have outlined a strategy for studying problems of number theory using quantum systems. The strategy consists of (i) reducing a number-theoretic statement to an assertion of the existence of an uninterrupted arithmetic subsequence in a sequence of numbers followed by (ii) finding a quantum system with an energy spectrum proportional to the latter. The existence of an arithmetic sub-series is illustrated by a cascade of resonant transitions under a periodic perturbation.

In this spirit, we have studied the example of the closeness of the set of natural numbers under multiplication in great detail. In doing so, we identified a difficulty that may occur in several instances of our class of protocols: the hopping constants in the resulting resonance cascades exhibit a sharp dependence on the site number. As a result, the eigenstates become localized inhibiting mobility along the energy axis. Subsequently, we found a way to unlock the mobility, so far in the downward direction only. The recipe calls for introducing a few specifically designed short “windows of silence” during which the perturbation is turned off. Hence this protocol requires, as the starting point, the preparation of an excited state of the potential. Such preparation could be performed using quantum optimal control methods like those presented in Sec. II B. Due to the logarithmic scaling of the energy levels (which leads to continuum-like behavior at higher levels but relatively large energy spacings between, e.g., the ground and first excited state), we found that gradient-based methods like GRAPE [15] tend to fail. On the other hand, gradient-free methods like genetic algorithms or methods relying on the constrained optimization within a given basis, like the the CRAB [28] or GROUP [29] methods will likely succeed, and both methods have been shown to work for similar atomic state preparation problems [30, 31].

In future, we plan to work on designing schemes in

which one starts from the ground state of the trap and ignites a resonance cascade propagating upward in energy. In this regard, preliminary results have been shown in related work [32]. We envisage that this will make a future experimental implementation easier. Experimentally, it is easier to prepare an atom in the ground state than in a well defined excited state. Moreover, an upward oriented resonance cascade may be readily detectable by counting atoms that leave the trap completely, as they reach the threshold between the bound and the continuous spectra. Hence atom loss would be a clear experimental signature of an interrupted cascade.

ACKNOWLEDGMENTS

HK and CW wish to acknowledge the computational facilities of the Advanced Computing Research Centre, University of Bristol - <http://www.bris.ac.uk/acrc/>. MO was supported by the NSF Grant No. PHY-1912542. OVM acknowledges the support by the DLR German Aerospace Center with funds provided by the Federal Ministry for Economic Affairs and Energy (BMWi) under Grant No. 50WM1957 and No. 50WM2250E. The authors would like to thank the Institut Henri Poincaré (UAR 839 CNRS-Sorbonne Université) and the LabEx CARMIN (ANR-10-LABX-59-01) for their support. - and the Institut Henri Poincaré (UAR 839 CNRS-Sorbonne Université) and LabEx CARMIN (ANR-10-LABX-59-01). GM and AT thank the kind hospitality and support from the program "Out-of-equilibrium Dynamics and Quantum Information of Many-body Systems with Long-range Interactions" at KITP (Santa Barbara). GM acknowledges the grants PNRR MUR Project PE0000023-NQSTI and PRO3 Quantum Pathfinder.

A significant portion of this work was produced during the thematic trimester on "Quantum Many-Body Systems Out-of-Equilibrium", at the Institut Henri Poincaré (Paris): AT, GM, and MO are grateful to the organizers of the trimester, Rosario Fazio, Thierry Giamarchi, Anna Minguzzi, and Patrizia Vignolo, for the opportunity to be a part of the program.

Appendix A: The $\ln(n)$ -spectrum potential: matrix elements of the perturbation

In this article, we are concerned with a design of an experimental protocol that can make the existence of equidistant energy level ladders visible. Our method of choice is study of mobility along the energy axis under a resonant perturbation. The design process involves analyzing simple numerical and analytic models of the process: this appendix and the ones that follow are devoted to that goal.

In the main text, we suggest using a parametric drive for inducing a resonance cascade. In particular, given the

potential $U(x)$ that produces a logarithmic spectrum (3),

$$\begin{aligned}\hat{H} &= \frac{\hat{p}^2}{2m} + U^L(x) \\ \hat{H}|n\rangle &= E_n|n\rangle \\ E_n &= U_0 \ln(n) \\ n &= 1, 2, 3, \dots,\end{aligned}$$

we apply a perturbation

$$V(x, t) = \epsilon \cos(\Omega t) U^L(x),$$

where

$$\Omega = U_0 \ln(\tilde{n}),$$

and \tilde{n} is a natural number. Note also that in the main text, we supplement the $\cos(\Omega t)$ time dependence of the perturbation with a few quarter-period-long windows of silence, as a method to enhance the mobility along the energy axis.

In the view of the above, estimates for the matrix elements of the potential,

$$\langle n'|U^L|n\rangle$$

will become needed. These estimates are the goal of this appendix.

1. A logarithmic approximation to the $\ln(n)$ -spectrum potential

In classical mechanics, the solution to the problem of restoring a trapping potential from its frequency as a function of energy is well-known [33]:

$$x(U) = \frac{1}{\sqrt{2m}} \int_{U(0)}^U \frac{dE}{\omega(E)\sqrt{U-E}},$$

where $\omega(E)$ is the oscillation frequency as a function of energy, $x(U)$ is the inverse of the potential function $U(x)$ for $x \geq 0$, $U(0)$ is the value of the potential at the origin, and the potential $U(x)$ is assumed to be an even function of x : $U(-x) = U(x)$. On the other hand, given a quantum energy spectrum, E_n , the classical frequency can readily be extracted:

$$\omega = \frac{1}{\hbar} \frac{dE_n}{dn}. \quad (\text{A1})$$

In our case, the spectrum E_n is given by (3). Then the classical frequency as a function of energy becomes

$$\omega = \frac{1}{\hbar} U_0 e^{-\frac{E}{U_0}}. \quad (\text{A2})$$

Now, assuming $U_0 = -\infty$, we get (4). The insert in Fig. 7(a) shows a good agreement between the quantum $\ln(n)$ -spectrum potential and its classical counterpart everywhere except for the substantially quantum region $|x| \lesssim a$ (whose size is comparable to the spatial extent of the quantum ground state).

2. Classical motion in a logarithmic potential

Classical equations of motion generated by the Hamiltonian

$$H_{\text{cl}}^{\text{L}} = \frac{p^2}{2m} + U_{\text{cl}}^{\text{L}}(x) ,$$

with $U_{\text{cl}}^{\text{L}}(x)$ given by (4), can be readily solved, albeit implicitly:

$$t = \pm T(E) \begin{cases} +\frac{1}{4} \operatorname{erf} \left(\sqrt{\ln \left(\frac{b(E)}{x} \right)} \right) & \text{for } x > 0 \\ -\frac{1}{4} \operatorname{erf} \left(\sqrt{\ln \left(\frac{-b(E)}{x} \right)} \right) + \frac{1}{2} & \text{for } x < 0 \end{cases} , \quad (\text{A3})$$

where $T(E) = (2\pi)/\omega(E)$ is the classical period, $\omega(E)$ is the classical frequency given by (A2), and

$$b(E) = \sqrt{\frac{\pi}{2}} a e^{\frac{E}{V_0}}$$

(see Fig. 11). At $t = \pm \frac{T}{4}$ particle's trajectory experiences

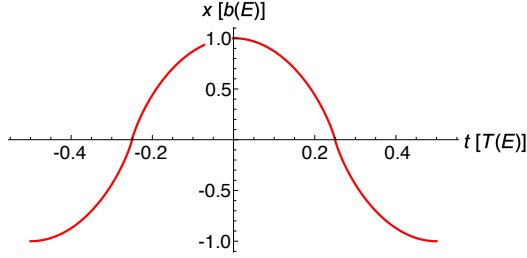


FIG. 11. **Classical trajectory in a logarithmic potential.**

The time dependence of the coordinate is given by a universal function (A3), with the time and coordinate properly rescaled in terms of the period $T(E)$ and the amplitude $b(E)$. Note that the $x(t)$ curve experience a singularity at $t = \pm \frac{T}{4}$ where velocity diverges logarithmically. It is hard to identify in a plot.

a logarithmic singularity:

$$t \mp \frac{T}{4} \approx \mp \frac{T}{4\sqrt{\pi}} \frac{x}{b \sqrt{\ln \left(\frac{b}{|x|} \right)}} . \quad (\text{A4})$$

In the vicinity of these singularities, the implicit relations (A4) can be approximately inverted, using sequential iterations:

$$\begin{aligned} x_{n+1} &= \mp 4\sqrt{\pi} b \left(\frac{t \mp \frac{T}{4}}{T} \right) \sqrt{\ln \left(\frac{b}{|x_n|} \right)} \\ x_0 &= \mp 4\sqrt{\pi} b \left(\frac{t \mp \frac{T}{4}}{T} \right) \end{aligned}$$

A comparison between the x_1 and x_2 iterations shows that

$$x(t) \approx x_1(t) = \mp 4\sqrt{\pi} b \left(\frac{t \mp \frac{T}{4}}{T} \right) \sqrt{\ln \left(\frac{T}{4\sqrt{\pi}(t \mp \frac{T}{4})} \right)} , \quad (\text{A5})$$

constitutes an accurate approximation to the true trajectory if

$$\sqrt{\ln \left(4\sqrt{\pi} \left(t \mp \frac{T}{4} \right) \right)} \ll \frac{T}{4\sqrt{\pi} \left(t \mp \frac{T}{4} \right)} ;$$

this condition is satisfied for

$$t \mp \frac{T}{4} \ll 0.1 \times T .$$

In addition, let us observe the following. (a) The asymptotic expansion of the erf-function,

$$\operatorname{erf}(y) \stackrel{y \gg 1}{\approx} 1 - e^{-y^2} \left\{ -\frac{1}{\sqrt{\pi}y} + \frac{1}{2\sqrt{\pi}y^3} + \mathcal{O}\left(\frac{1}{y^5}\right) \right\} ,$$

shows that the approximation (A4) is valid for

$$\ln \left(\frac{b}{|x|} \right) \gtrsim \frac{1}{2} .$$

(b) On the other hand, the logarithmic singularity in the classical potential (4) is regularized in the quantum case (Fig. 7(a)), at $|x| \sim a$. This cut-off introduces the following bound:

$$\ln \left(\frac{b}{|x|} \right) \lesssim n ,$$

n being the typical eigenstate index of interest. In our case, $3 \lesssim n \lesssim 27$.

Observe that in (A4), another constant b , outside of the logarithm, depends on n exponentially. Accordingly, in these estimates, we will replace the logarithm appearing in (A4) by a constant L :

$$\begin{aligned} \ln \left(\frac{b}{|x|} \right) &\rightarrow L \\ \frac{1}{2} &\lesssim L \lesssim 27 \end{aligned} . \quad (\text{A6})$$

Interestingly, in the estimates that follow, the actual value of the constant L turns out to be irrelevant.

As it follows from our derivation below, the singularity (A4) controls the behavior of the quantum off-diagonal matrix elements of the potential energy, for large differences between the quantum numbers.

3. Semiclassical approximation for the off-diagonal matrix elements of coordinate-dependent observables in one-dimensional traps: general results

In [34], one can find a set of results on a semiclassical approximation for off-diagonal matrix elements of quantum observables, both for the case of two close energies (§48), and for two energies far apart (§51). Before we address the question of the matrix elements of the potential energy $U^L(x)$ that generates the $\ln(n)$ spectrum (3), we will restate the main results in the former limit (shown to be relevant to our case), focussing on the case where the observable is a function of a coordinate.

Consider a one-dimensional quantum potential well with a potential energy $U(x)$. Let $\hat{A} = A(x)$ be the observable of interest. We will be interested in a semiclassical approximation to the matrix elements of the observable,

$$\langle n' | \hat{A} | n \rangle,$$

where $|n\rangle$ are the eigenstates of the system; the corresponding eigenenergies are E_n .

In the classically allowed region, $E \geq U(x)$, the semiclassical approximation to eigenstate wavefunction is

$$\psi_n(x) = \frac{2}{\sqrt{T(E_n)v(x, E_n)}} \cos\left(\frac{1}{\hbar} \int_{x_1(E_n)}^x p(x', E_n) dx' - \frac{\pi}{4}\right) \quad (\text{A7})$$

where $T(E) = 2\pi/\omega(E)$ is the classical oscillation period as a function of energy, $\omega(E)$ is the classical frequency,

$$p(x, E) \equiv \sqrt{2m(E - U(x))}$$

is the magnitude of the classical momentum as a function of coordinate and energy, $v(x, E) \equiv p(x, E)/m$ is the magnitude of the classical velocity, and $x_1(E)$ is the left turning point of particle's trajectory. i.e. the smallest of the two solutions of an algebraic equation $U(x) = E$. Within the accuracy of the semiclassical approximation, the wavefunction (A7) is normalized to unity. More specifically, its normalization integral become a unity if one replaces $\cos^2(\dots)$ appearing there by $\frac{1}{2}$.

Introduce an energy E close to each of the energies E_n and $E_{n'}$:

$$E \approx E_n, E_{n'}$$

A concrete choice for this energy is, to the leading order of the semiclassical approximation, irrelevant. A choice $E = E_n$ will make the quantum-classical relationship more elegant; another choice, $E = (E_n + E_{n'})/2$ may improve accuracy beyond the leading order [35]; it also preserves the Hermiticity of the matrix for the given observable. In this text, we will not commit to any particular convention.

For a matrix element of an observable $A(x)$, between an eigenstate $|n'\rangle$ and an eigenstate $|n\rangle$, we get:

$$\begin{aligned} \langle n' | \hat{A} | n \rangle &= \int_{-\infty}^{+\infty} dx A(x) \psi_{n'}(x) \psi_n(x) \\ &\approx \frac{4}{T(E)} \int_{x_1(E)}^{x_2(E)} \frac{dx}{v(x, E)} A(x) \cos\left(\frac{1}{\hbar} \int_{x_1(E_{n'})}^x p(x', E_{n'}) dx' - \frac{\pi}{4}\right) \cos\left(\frac{1}{\hbar} \int_{x_1(E_n)}^x p(x'', E_n) dx'' - \frac{\pi}{4}\right) \\ &\approx \frac{2}{T(E)} \int_{x_1(E)}^{x_2(E)} \frac{dx}{v(x, E)} A(x) \cos\left(\int_{x_1(E)}^x dx' (p(x, E_{n'}) - p(x, E_n))\right) \\ &\approx \frac{2}{T(E)} \int_{x_1(E)}^{x_2(E)} \frac{dx}{v(x, E)} A(x) \cos\left(\frac{1}{\hbar} \int_{x_1(E)}^x dx' (p(x', E_{n'}) - p(x', E_n))\right) \\ &\approx \frac{2}{T(E)} \int_{x_1(E)}^{x_2(E)} \frac{dx}{v(x, E)} A(x) \cos\left(\int_{x_1(E)}^x \frac{dx'}{v(x, E)} \omega(E) (n' - n)\right) \\ &= \frac{2}{T(E)} \int_{t_1}^{t_1 + \frac{T(E)}{2}} dt A(x(t)) \cos((t - t_1)\omega(E)(n' - n)) \\ &= \frac{1}{T(E)} \int_{t_1}^{t_1 + \frac{T(E)}{2}} dt A(x(t)) \cos((t - t_1)\omega(E)(n' - n)) + \frac{1}{T(E)} \int_{t_1}^{t_1 + \frac{T(E)}{2}} dt A(x(t)) \cos((t - t_1)\omega(E)(n' - n)) \\ &= \frac{1}{T(E)} \int_{t_1}^{t_1 + \frac{T(E)}{2}} dt A(x(t)) \cos((t - t_1)\omega(E)(n' - n)) + \frac{1}{T(E)} \int_{t_1 - \frac{T(E)}{2}}^{t_1} dt A(x(t)) \cos((t - t_1)\omega(E)(n' - n)) \end{aligned} \quad (\text{A8})$$

Above, a semiclassical regime, where the potential $U(x)$

does not change appreciably on the scale of the de Broglie

wavelength, $\lambda_{d-B} \sim \hbar/p$, is assumed; we also used the relationship (A1). Here and below, t_1 is the instance of time when the particle reaches the left turning point, where $x(t_1) = x_1$. We also used $dt = dx/v(x, E)$. Finally, we used the fact the functions $A(x(t))$ and $\cos((n' - n)\omega(E)(t - t_1))$ are even with respect to a $(t - t_1) \rightarrow -(t - t_1)$ substitution and periodic with a period $T(E)$. We arrive at the familiar ([34]) semiclassical expression for the matrix elements of a coordinate-dependent observable $A(x)$ between two close energy levels:

$$\begin{aligned} \langle n' | \hat{A} | n \rangle &\approx \frac{1}{T(E)} \int_{-\frac{T(E)}{2}}^{+\frac{T(E)}{2}} d\tau A(x(t_1 + \tau)) \cos(\Delta n \omega(E)\tau) \\ &\approx \frac{(-1)^{\Delta n}}{T(E)} \int_{-\frac{T(E)}{2}}^{+\frac{T(E)}{2}} d\tau' A(x(t_2 + \tau')) \cos(\Delta n \omega(E)\tau'). \end{aligned} \quad (\text{A9})$$

$$(\text{A10})$$

Under this approximation, the matrix element in question becomes a cosine Fourier component of the time dependence of the classical counterpart. Here

$$\begin{aligned} \Delta n &= n' - n \\ E &\approx E_n, E_{n'} \\ t_1 &= \text{left turning point instance} \\ t_2 &= \text{right turning point instance} \\ \omega(E) &= \text{frequency at energy } E. \end{aligned}$$

Note that for this choice of the lower bound of the Fourier integral, the corresponding sinus Fourier component vanishes.

4. Off-diagonal matrix elements of the potential energy for the $\ln(n)$ -spectrum potential

In this subsection we are going to use the semi-classical formula (A10) to estimate off-diagonal matrix elements of the potential energy $|\langle n' | U^L | n \rangle|$, in conditions where the quantum number difference $n' - n$ is large as compared to unity (so that the existing intuition for asymptotic expansions of Fourier integrals [36] is applicable), but small as compared to n (that ensures that the formula (A10) is still valid). Within the accuracy of the semiclassical approximation, we can replace the $\ln(n)$ -spectrum potential (3) with its classical counterpart (4). The classical trajectory is given by (A3).

According to [36], at large orders of a Fourier expansion, the Fourier components are dominated by the singularities in the time-dependence. In our case, we are dealing with logarithmic singularities. Indeed substituting the approximation (A5) to the potential (4) and

using the substitution (A6), one gets

$$U_{cl}^L(x(t)) \stackrel{t \approx \mp \frac{T}{4}}{\approx} U_0 \ln \left(4\sqrt{2} \left(\frac{b}{a} \right) \sqrt{L} \left(\frac{|t \mp \frac{T}{4}|}{T} \right) \right). \quad (\text{A11})$$

To estimate the Fourier integral (A10) at large quantum number differences ($1 \ll |n' - n| \ll n$), we extend the integral to the full axis of time, use the approximation (A11), and introduce an ultraviolet cut-off, shown later to be removable. The following integral emerges:

$$\lim_{\lambda \rightarrow 0} \int_{-\infty}^{+\infty} d\tau \exp(i\tilde{\Omega}\tau) \exp(-\lambda|\tau|) \ln(\sigma|\tau|) = -\frac{\pi}{|\tilde{\Omega}|}.$$

The following estimate for the off-diagonal matrix elements of the potential ensues:

$$\langle n' | U^L | n \rangle \stackrel{|n' - n| \gg 1}{\approx} \begin{cases} (-1)^{\frac{n' - n}{2} - 1} \frac{U_0}{n' - n} & \text{for } n' - n = \text{even} \\ 0 & \text{for } n' - n = \text{odd} \end{cases}. \quad (\text{A12})$$

A comparison with the numerical results (Fig. 12) shows that while the formula (A12) does capture the overall scaling,

$$|\langle n' | U^L | n \rangle| \stackrel{|n' - n| \gg 1}{\approx} A \frac{U_0}{|n' - n|}, \quad (\text{A13})$$

it overestimates the coefficient A by 25%, predicting that $A = 1$ instead of the numerical $A = 0.80$ (Fig. 9(a)).

5. Diagonal matrix elements of the potential energy

For completeness, let us present the semiclassical approximation for the diagonal matrix elements of the potential energy.

Again, within the accuracy of the semiclassical approximation, we can replace the $\ln(n)$ -spectrum potential (3) with its classical counterpart (4).

Generally, diagonal matrix elements of observables are approximated using classical temporal averages. In our case however, a virial theorem that has been previously applied to a logarithmic potential ([37]) allows to avoid the temporal average integrals: using the result obtained in [37], we get:

$$\langle n | U^L | n \rangle \approx U_0 \ln \left(e^{-\frac{1}{2}} n \right). \quad (\text{A14})$$

Fig. 9(b) shows an excellent agreement between our prediction and ab initio results for a $\ln(n)$ -spectrum potential with $N_b = 120$ bound states.

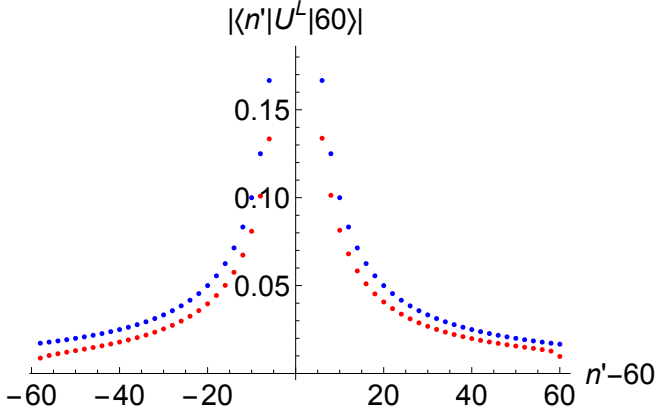


FIG. 12. **A more complete presentation of the off-diagonal matrix elements of the perturbation (again, represented, in the case of a parametric excitation, by the potential energy).** This Figure contains information that is supplementary to the one presented at Fig. 9(a). Here, the full information about the sign the quantum number differences $n' - n$ is given. Only even values of $n' - n$ are represented, since the odd values vanish due to the parity selection rule. The red dots represent numerical results. The $\ln(n)$ -spectrum potential used had $N_b = 120$ bound states. We also present the theoretical prediction (A12) that contains no fit parameters (blue dots).

Appendix B: The exponential lattice

The goal of this appendix is to develop a theory for a quantum infinite one-dimensional lattice whose hopping coefficient decays exponentially in space. We found that this model is relevant to the problem of a parametric excitation of the $\ln(n)$ -spectrum potential. In particular, using the exponential lattice model, we were able to identify the source of a localization in the space of the unperturbed eigenstates and devise the ways to break such a localization. The map between the two models is given in Subsec. B 6.

Consider the following one-body Hamiltonian:

$$\hat{H}_{\text{EL}} = -J_0 \sum_{m=-\infty}^{+\infty} e^{-\gamma m} (|m+1\rangle\langle m| + |m\rangle\langle m+1|) , \quad (\text{B1})$$

where m are the lattice site indices, and γ is a positive constant. Below, we will discuss the solutions to the time-independent Schrödinger equation,

$$-J_0 e^{-\gamma m} (e^{\gamma} \psi_{m-1} + \psi_{m+1}) = E \psi_m , \quad (\text{B2})$$

$$m = 0, \pm 1, \pm 2, \dots$$

where ψ_m is the coordinate representation of an eigenstate

$$|\psi\rangle = \sum_{m=-\infty}^{+\infty} \psi_m |m\rangle$$

of an energy E :

$$\hat{H}_{\text{EL}}|\psi\rangle = E|\psi\rangle .$$

For the reasons that will become clear below, we have to start our discussion not from the eigenenergies but from the $m \rightarrow -\infty$ behavior of the eigenstates. We will proceed to the analysis of the spectrum, followed by the $m \rightarrow +\infty$ asymptotic behavior.

1. Eigenfunctions in the “dark state” region, $m \rightarrow -\infty$

Consider an eigenstate $|\psi\rangle$ of an energy E . At

$$m \ll \frac{1}{\gamma} \ln \left(\frac{J_0}{|E|} \right) ,$$

where

$$|E| \ll J_m ,$$

coefficients in front of the wavefunction components $\psi_{m\pm 1}$ in the Schrödinger equation (B2) exponentially explode, reducing the problem to finding the kernel (i.e. the “dark states” (DS) [22, 23]) of the Hamiltonian (B1):

$$\hat{H}_{\text{EL}}|\psi_{\text{DS}}\rangle = 0 , \quad (\text{B3})$$

or

$$e^{\gamma} (\psi_{\text{DS}})_{m-1} + (\psi_{\text{DS}})_{m+1} = 0$$

$$m = m_{\text{DS}}, m_{\text{DS}} - 1, m_{\text{DS}} - 2, \dots . \quad (\text{B4})$$

Here and below, m_{DS} is the (right) boundary of the zone of validity of the “dark state” approximation (B4), and

$$J_m \equiv J_0 e^{-\gamma m} .$$

The wave function $(\psi_{\text{DS}})_m$ can be immediately found:

$$\psi_m \stackrel{m \rightarrow -\infty}{\approx} (\psi_{\text{DS}})_m$$

$$(\psi_{\text{DS}})_m = \begin{cases} (-1)^{\frac{m_{\text{DS}}-m}{2}} e^{-\gamma \frac{m_{\text{DS}}-m}{2}} \psi_{m_{\text{DS}}} & \text{for } m - m_{\text{DS}} = \text{even} , \\ 0 & \text{for } m - m_{\text{DS}} = \text{odd} \end{cases} ,$$

$$m = m_{\text{DS}}, m_{\text{DS}} - 1, m_{\text{DS}} - 2, \dots \quad (\text{B5})$$

where $\psi_{m_{\text{DS}}}$ is the value of the *exact* eigenfunction at m_{DS} , presumed to be known. Expectedly, in terms of constant hopping lattices this state can be interpreted a superposition of the two zero energy plane waves with momenta $\pm \frac{\pi}{2}$.

Note the following however. As m tends to the negative infinity, the wavefunction (B5) decays as $e^{\gamma \frac{m}{2}}$, while the matrix elements of the Hamiltonian (B1) explode in a much faster fashion, i.e. as $e^{-\gamma m}$. The only reason why the energy of the eigenstate does not diverge is the destructive interference between the two terms in the equation (B4).

Imagine now that one decides to truncate the lattice at some negative position m_{left} , in such a way that the allowed values of the coordinate m now span the range: $m = m_{\text{DS}}, m_{\text{DS}}-1, m_{\text{DS}}-2, \dots, m_1+1, m_{\text{left}}$. The norm

$$\hat{H}_{\text{EL}}|\psi_{\text{DS}}\rangle = -J_0 e^{-\gamma m_{\text{left}}} (-1)^{\frac{m_{\text{DS}}-(m_{\text{left}}+1)}{2}} e^{-\gamma \frac{m_{\text{DS}}-(m_{\text{left}}+1)}{2}} \psi_{m_{\text{DS}}} \propto e^{+\gamma \frac{|m_{\text{left}}|}{2}},$$

unless m_{left} and m_{DS} have the same parity:

$$m_{\text{DS}} - m_{\text{left}} = \text{even} . \quad (\text{B6})$$

We arrive at the following conclusion: in the problem at hand, extending our lattice to $m = -\infty$ may produce unphysical eigenstates. Hence, we suggest the following amendment to our model. We will continue being interested in the eigenstates that are localized far away from the left boundary m_{left} , rendering the actual position of it irrelevant. However, the *parity* of m_{left} will remain important. Without loss of generality, we may assume that

$$m_{\text{left}} = \text{even} .$$

Finally, using (B6) establish the following rule: the infinite lattice solutions of the Schrödinger equation (B2) must be *post-selected* in such a way that only the eigenstates with the “dark state” asymptotic behavior (B5) where

$$m_{\text{DS}} = \text{even} . \quad (\text{B7})$$

are kept. This rule plays an important role in the next subsection.

2. The $+E \leftrightarrow -E$ symmetry, translational invariance, and the energy spectrum

Consider the Schrödinger equation (B2). Two properties of the spectrum can be proven.

Property B.1 (Positive-negative energy parity). *Let $\psi_m^{(+)}$ be a solution of the eigenvalue problem (B2) corresponding to an eigenenergy $E = E^{(+)}$. Then the eigenstate-eigenenergy pair*

$$\begin{aligned} \psi_m^{(-)} &= (-1)^m \psi_m^{(+)} \\ E &= E^{(-)} = -E^{(+)} . \end{aligned} \quad (\text{B8})$$

is also a solution of (B2). The statement will remain valid if the infinite lattice is reduced to a ray or a line segment bounded by a Dirichlet boundary condition.

of the wavefunction (B5) converges to a finite value for $m_{\text{left}} \rightarrow -\infty$. Hence in this limit, the wavefunction (B5) remains finite. However, in the same limit, the left hand side of the equation (B3) will exponentially explode,

Proof. Indeed, substituting $\psi_m^{(-)}$ to (B2), we get

$$\begin{aligned} &-J_0 e^{-\gamma m} \left(e^{\gamma} \psi_{m-1}^{(-)} + \psi_{m+1}^{(-)} \right) \\ &\stackrel{(\text{B8})}{=} -J_0 e^{-\gamma m} \left(e^{\gamma} (-1)^{m-1} \psi_{m-1}^{(+)} + (-1)^{m+1} \psi_{m+1}^{(+)} \right) \\ &= -J_0 e^{-\gamma m} (-1) (-1)^m \left(e^{\gamma} \psi_{m-1}^{(+)} + \psi_{m+1}^{(+)} \right) \\ &\stackrel{(\text{B2})}{=} (-1) (-1)^m E^{(+)} \psi_m^{(+)} \\ &\stackrel{(\text{B8})}{=} E^{(-)} \psi_m^{(-)} . \end{aligned}$$

□

Property B.2 (Translational invariance). *Let $\psi_m^{(\Delta m=0)}$ be a solution of the eigenvalue problem (B2) corresponding to an eigenenergy $E = E^{(\Delta m=0)}$. Then the eigenstate-eigenenergy pair*

$$\begin{aligned} \psi_m^{(\Delta m)} &= \psi_{m-\Delta m}^{(\Delta m=0)} \\ E &= E^{(\Delta m)} = e^{-\gamma \Delta m} E^{(\Delta m=0)} . \end{aligned} \quad (\text{B9})$$

is also a solution of (B2).

Proof. Again, substituting $\psi_m^{(\Delta m)}$ to (B2), we get

$$\begin{aligned} &-J_0 e^{-\gamma m} \left(e^{\gamma} \psi_{m-1}^{(\Delta m)} + \psi_{m+1}^{(\Delta m)} \right) \\ &\stackrel{(\text{B9})}{=} -J_0 e^{-\gamma m} \left(e^{\gamma} \psi_{m-\Delta m-1}^{(\Delta m=0)} + \psi_{m-\Delta m+1}^{(\Delta m=0)} \right) \\ &= -J_0 e^{-\gamma \Delta m} e^{-\gamma(m-\Delta m)} \left(e^{\gamma} \psi_{m-\Delta m-1}^{(\Delta m=0)} + \psi_{m-\Delta m+1}^{(\Delta m=0)} \right) \\ &\stackrel{(\text{B2})}{=} e^{-\gamma \Delta m} E^{(\Delta m=0)} \psi_{m-\Delta m}^{(\Delta m=0)} \\ &\stackrel{(\text{B9})}{=} E^{\Delta m} \psi_m^{(\Delta m)} . \end{aligned}$$

□

The Property B.2 may seem paradoxical at first, as it may seem to imply, in combination with the Property B.1 that there are twice as many eigenstates of the Hamiltonian as there are lattice sites. This apparent paradox is resolved in Subsection B.1. As we show there, a model (B1) on an infinite lattice is not physical, as it is not a limit of a problem on a ray of sites to the right of a Dirichlet boundary. However an infinite lattice model where the eigenstates are post-selected in such a way that

only the states that in the limit $m \rightarrow -\infty$ develop nodes at the *odd* sites are kept represents a faithful

$$\begin{aligned} m_{\text{left}} &\rightarrow -\infty \\ m_{\text{left}} &= \text{even} \end{aligned}$$

limit of a ray with a Dirichlet boundary at m_{left} . More precisely, we assume a

$$\psi_{m_{\text{left}}-1} = 0$$

condition at the $(m_{\text{left}} - 1)$ 'th site. This consideration leads to the following amendment to the Property B.2:

$$\Delta m = \text{even} . \quad (\text{B10})$$

3. Eigenfunctions in the ‘‘classically forbidden’’ region, $m \rightarrow +\infty$

In this subsection, we will be interested in the region of space where

$$|E| \gg J_m \quad (\text{B11})$$

or

$$m \gg \frac{1}{\gamma} \ln \left(\frac{J_0}{|E|} \right) . \quad (\text{B12})$$

If one forgets about the spatial dependence of J_m for a moment, this area of space corresponds to a ‘‘classically forbidden region’’ (CF) where no waves can propagate. One would expect the wavefunction to develop an exponentially decaying tail instead.

Furthermore, we will assume that the spatial dependence of the hopping coefficient is slow in comparison with the spatial dependence of the eigenstates. This is a domain of the parameter space where a semiclassical approximation [34] can be used. We will verify the validity of this assumption a posteriori.

Consider first the case of

$$E > 0 .$$

If the hopping coefficient were a constant (let's call it \bar{J}), then the exponentially decaying solution of the Schrödinger equation (B2) would have a form

$$(\psi_{J_m = \bar{J}})_m = (-1)^{m-m_{\text{CF}}} e^{-\bar{\kappa}m} \psi_{m_{\text{CF}}} , \quad (\text{B13})$$

where m_{CF} is the (left) boundary of the area of validity of the ‘‘classically forbidden region’’ approximation, $\psi_{m_{\text{CF}}}$ is the value of the *exact* eigenfunction at m_{CF} , and

$$\bar{\kappa} = \text{arccosh} \left(\frac{E}{2\bar{J}} \right) \Big|_{|E| \gg \bar{J}} \approx \ln \left(\frac{E}{\bar{J}} \right) .$$

In the first order of the semiclassical approximation [34], the $\bar{\kappa}m$ under the exponent in (B13) is modified as

$$\bar{\kappa}m \rightarrow \sum_{m'=m_{\text{CF}}}^{m-1} \kappa_{m'} ,$$

with $\kappa_m \equiv \ln \left(\frac{E}{J_m} \right)$. After a straightforward manipulation (see Subsection B 4 for details), we get the following $m \rightarrow +\infty$ approximation (still restricted to positive energies, $E > 0$):

$$\psi_m \stackrel{m \rightarrow +\infty}{\approx} (\psi_{\text{CF}})_m$$

$$(\psi_{\text{CF}})_m = (-1)^{m-m_{\text{CF}}} \left(\frac{\sqrt{J_{m_{\text{CF}}} J_{m-1}}}{E} \right)^{m-m_{\text{CF}}} \psi_{m_{\text{CF}}} .$$

$$\begin{aligned} m &= m_{\text{CF}}, m_{\text{CF}} + 1, m_{\text{CF}} + 2, \dots \\ E &> 0 \end{aligned}$$

The case of negative energies,

$$E < 0 ,$$

can be evaluated in a similar fashion: the only difference between the two signs of energies being that at the negative energies, there is no sign-alternating factor in the expression analogous to (B13).

Finally, an expression that covers both signs of energy reads

$$\begin{aligned} \psi_m &\stackrel{m \rightarrow +\infty}{\approx} (\psi_{\text{CF}})_m \\ (\psi_{\text{CF}})_m &= \left\{ \begin{array}{ll} (-1)^{m-m_{\text{CF}}} & \text{for } E > 0 \\ 1 & \text{for } E < 0 \end{array} \right\} \left(\frac{\sqrt{J_{m_{\text{CF}}} J_{m-1}}}{|E|} \right)^{m-m_{\text{CF}}} \psi_{m_{\text{CF}}} . \end{aligned} \quad (\text{B14})$$

$$\begin{aligned} m &= m_{\text{CF}}, m_{\text{CF}} + 1, m_{\text{CF}} + 2, \dots \\ &\text{both } E > 0 \text{ and } E < 0 \end{aligned}$$

Let us finally assess the validity of the semiclassical

approximation. According to [34], the semiclassical

approximation is valid when the de-Broglie wavelength, $\lambda_{\text{d-B}}$, does not change appreciably over a length comparable to itself:

$$\frac{d\lambda_{\text{d-B}}}{dm} \ll 1.$$

In our case,

$$\lambda_{\text{d-B}} \sim \frac{1}{\kappa_m} \sim \frac{1}{\gamma(m - \tilde{m})},$$

with $\tilde{m} = -\frac{1}{\gamma} \ln\left(\frac{|E|}{J_0}\right)$ is the location where the hopping coefficient is comparable to the magnitude of energy. The condition of validity of the approximation becomes

$$|E| \gg e^{\sqrt{\gamma}} J_m. \quad (\text{B15})$$

Notice that this condition is more restrictive than the condition for being in a classically forbidden region (B12).

4. Derivation of semiclassical formula (B14) for the eigenstate wavefunctions in the ‘‘classically forbidden’’ region

In this subsection we will derive the WKB approximation for the exponential lattice which leads to (B14). We will follow Bremmer’s method as described in [38]. Since in the classically forbidden region, the spatial dependence of the hopping coefficient is slow, we divide the domain of interest into regions, not necessarily of the same size, with an approximately constant J_n in each region. The right boundary of each region is labeled by n_j , and the difference in magnitudes between J_j in neighboring regions is small.

Now we consider the scattering problem with a step at n_j . The hopping coefficient to the left is J_L and to the right is J_R . To the right of the step the wavefunction is a decaying exponential with wavenumber κ_R , and to the left κ_L . The transmission coefficient is found to be

$$t_{n_j} = \frac{J_L(e^{\kappa_L} - e^{-\kappa_L})}{J_L e^{\kappa_L} - J_R e^{-\kappa_R}} e^{(\kappa_R - \kappa_L)n_j}.$$

To evaluate the wavefunction at some later point, we neglect reflection coefficients, which are very small in magnitude. We are free to choose the size of the regions in our domain, and more importantly their endpoints, so we may choose the endpoint of the final region, n_N , to be at the lattice point where we wish to evaluate the wavefunction. There, the wavefunction is approximated by

$$\psi_{n_N} = e^{-\kappa_{n_N+1} n_N} \times \prod_{j=0}^{N-1} \frac{J_{n_j}(e^{\kappa_{n_j}} - e^{-\kappa_{n_j}})}{J_{n_j} e^{\kappa_{n_j}} - J_{n_{j+1}} e^{-\kappa_{n_{j+1}}}} e^{(\kappa_{n_{j+1}} - \kappa_{n_j})n_j}.$$

Since the difference between neighboring J_n is small,

$$\frac{J_{n_j}}{J_{n_{j+1}}} = 1 + \epsilon_j, \quad |\epsilon_j| \ll 1.$$

Then, to first order in the ϵ_j ,

$$\frac{J_{n_j}(e^{\kappa_{n_j}} - e^{-\kappa_{n_j}})}{J_{n_j} e^{\kappa_{n_j}} - J_{n_{j+1}} e^{-\kappa_{n_{j+1}}}} = \sqrt{\frac{J_{n_j} \sinh \kappa_{n_j}}{J_{n_{j+1}} \sinh \kappa_{n_{j+1}}}},$$

which becomes a telescoping series when the product is taken leaving

$$\psi_{n_N} = \sqrt{\frac{J_{n_0} \sinh \kappa_{n_0}}{J_{n_{N-1}} \sinh \kappa_{n_{N-1}}}} e^{-\kappa_{n_{N+1}} n_N} \prod_{j=0}^{N-1} e^{(\kappa_{n_{j+1}} - \kappa_{n_j})n_j}.$$

The remaining exponential terms can be rewritten in terms of a sum, so that

$$\psi_{n_N} = \sqrt{\frac{J_{n_0} \sinh \kappa_{n_0}}{J_{n_{N-1}} \sinh \kappa_{n_{N-1}}}} e^{-n_0 \kappa_0 + \sum_{j=1}^{N-1} (n_{j-1} - n_j) \kappa_j}.$$

We can now restore the κ_j associated with particular lattice points, so the WKB approximation for the wavefunction at a particular lattice point m becomes

$$\psi_m = \sqrt{\frac{J_{m_0} \sinh \kappa_{m_0}}{J_{m-1} \sinh \kappa_{m-1}}} e^{-m_0 \kappa_0 - \sum_{j=1}^{m-1} \kappa_j}.$$

Next we invoke (B12), the condition that $|E| \gg J_m$. We consider propagation only within the classically forbidden region, so $m_0 = m_{cf}$, and the summation in the exponent is now

$$\sum_{j=m_{CF}}^{m-1} \kappa_j.$$

To first order in J_m/E , this reduces the expression for the wavefunction to

$$(\psi_{CF})_m = e^{-m_{CF} \kappa_{CF}} \left(\frac{J_0}{|E|} e^{-\gamma(m_{CF} + m - 1)/2} \right)^{m - m_{CF}},$$

which can be rewritten using the definition of J_m to read

$$(\psi_{CF})_m = \left(\frac{\sqrt{J_{m_{CF}} J_{m-1}}}{|E|} \right)^{m - m_{CF}} \psi_{m_{CF}}.$$

5. Numerically exact eigenstates and discussion

Figs 13 and 14 show results of a numerical diagonalization of the Hamiltonian (B1) on a lattice with 201 sites $m = 0, \pm 1, \pm 2, \dots, \pm 100$ with Dirichlet boundary conditions.

Parity of the coordinate of the leftmost site (i.e., the fact that -100 is an even number) effectuates the post-selection condition (B6). It can be reformulated as follows: our numerical procedure preserves only a half of the eigenstates of the infinite lattice, namely those whose nodes in the $m \rightarrow -\infty$ region are located in the *odd* lattice sites.

We considered two values of the coupling decay rate γ : $\gamma = 0.3$ and $\gamma = \ln(3) \approx 1.10$. In the first case, coupling decay is slow enough to ensure the validity of the approximation (B14). The second case corresponds to a lattice that is relevant to the problem in the main text.

Fig 13 shows energy spectra in both $\gamma = 0.3$ and $\gamma = \ln(3)$ cases.

First of all, we noticed that in both cases, values $E = +J_0$ and $E = -J_0$ belong to the spectrum. We were not able to support this observation with an analytic result.

Nest, we used the states $E = +J_0$ and $E = -J_0$ as a reference to deploy the prediction (B9)-(B10). In both cases, the agreement between the numerical results and the formula (B9)-(B10) is remarkable. We also confirmed the prediction of the spectrum being symmetric with respect to $+E \leftrightarrow -E$ transformation, (B8).

Fig 14 shows the $E = +J_0$ and $E = -J_0$ eigenstates, for both values of γ considered. Both the ‘‘dark state’’ ((B5)) and the ‘classically forbidden region’’ ((B14)) approximations work remarkably well. The validity of the approximation (B14) for the $\gamma = \ln(3)$ case was unexpected, given the validity condition (B15).

6. Relationship between the parameters of the exponential lattice model and the parameters $\ln(n)$ -spectrum potential

The relationship between the exponential lattice model and the problem of the parametrically excited $\ln(n)$ -spectrum potential is as follows:

$$\begin{aligned} |m\rangle &= |n = \tilde{n}^m\rangle \\ \gamma &= \ln(\tilde{n}) \\ J_0 &= \frac{1}{2}U_0 \frac{A}{(\tilde{n} - 1)} \end{aligned}, \quad (\text{B16})$$

where A is the fit coefficient in for the dependence of the off-diagonal matrix elements of the potential energy on the quantum number difference:

$$|\langle n' | U^L | n \rangle| \approx U_0 \frac{A}{|n' - n|}.$$

Recall that in our numerical model, $A \approx 0.8$ (Fig. 9(a)).

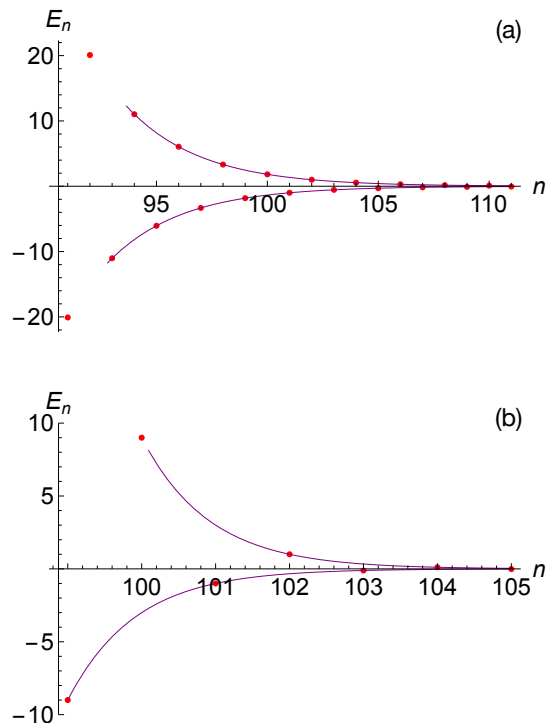


FIG. 13. **Exponential lattice: energy spectra.** The coupling constant decay rate is given by $\gamma = 0.3$ (a) and $\gamma = \ln(3)$ (b) respectively. Spectra are ordered in the descending order of the magnitude of energy. Energy is measured in the units of J_0 . Red dots is a numerical prediction. Solid thin lines represent the prediction (B9)-(B10). Notice also that for any magnitude of eigenenergy, both signs of the eigenenergy are present in the spectrum, in agreement with (B8). Finally, the presence of the $E = \pm J_0$ levels for both values of γ remains unexplained.

Appendix C: A conjecture that there exists an infinite number of even numbers whose Goldbach decomposition does not involve lower twin primes

In this section, we conjecture that there is an infinite number of even numbers w that feature the following property:

No lower twin (NLT) property For any of the Goldbach decompositions of w , $w = p_1 + p_2$, both $p_1 + 2$ and $p_2 + 2$ are composite numbers.

Note that unlike in the main text, here we *don't assume* that p_1 and p_2 stand in any particular order with respect to each other.

In preparation, let us reiterate a well-known result that there don't exist triplets of consecutive (separated by 2) primes unless the lower member of the triplet is 3. We will need, however, a stronger version of this statement

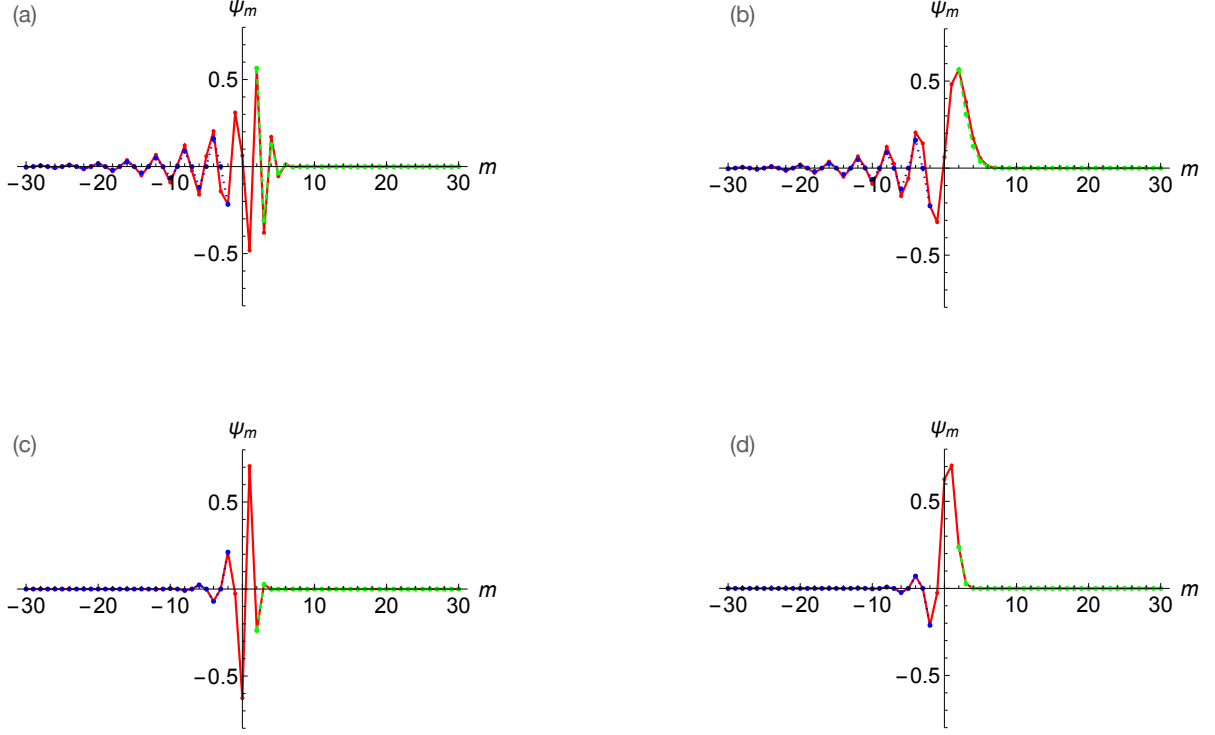


FIG. 14. **Exponential lattice: eigenstates.** The $E = +J_0$ ((a) and (c)) and $E = -J_0$ ((b) and (d)) eigenstates of the $\gamma = 0.3$ ((a) and (b)) and $\gamma = \ln(3)$ ((c) and (d)) lattices. The rest of the eigenstates are translations of the ones presented, by an even number of sites. Red circles and red solid lines are numerical results. Blue circles and blue dotted lines correspond to the “dark state” approximation (B5). Green circles and green dashed lines correspond to the “classically forbidden region” approximation (B14).

expressed in this

Lemma C.1. *Any lower twin prime p greater than 3 the following is true:*

$$p \equiv 2 \pmod{3}$$

Proof. First of all, since p is a prime different from 3,

$$p \equiv 1 \text{ or } 2 \pmod{3} .$$

Secondly, since $p + 2$ is also a prime different from 3,

$$p \equiv 2 \text{ or } 0 \pmod{3} .$$

Combining the two we get,

$$p \equiv 2 \pmod{3} .$$

□

We will also need the following

Lemma C.2. *All the evens w such that*

- (a) $w - 3 \neq \text{prime}$
- (b) $w \equiv 2 \pmod{6}$

possess the NLT property.

For example:

$$\begin{aligned} 38 &= 6 \times 6 + 2 = 2 \pmod{6} \\ 38 - 3 &= 35 = 5 \times 7 \neq \text{prime} \\ 38 &= 7 + 31 = 19 + 19 \\ 7 + 2 &= 9 = 3 \times 3 \neq \text{prime} \\ 31 + 2 &= 33 = 3 \times 11 \neq \text{prime} \\ 19 + 2 &= 21 = 3 \times 7 \neq \text{prime} \end{aligned}$$

Proof. Consider a Goldbach partition of w ,

$$w = p_1 + p_2 .$$

From the premise (a) it follows that

$$\begin{aligned} p_1 &\neq 3 \\ p_2 &\neq 3 \end{aligned} \tag{C1}$$

This can be proven using *reductio ad absurdum*. Assume that $p_2 = 3$. Then

$p_1 = w - p_2 = (w - 3) + (3 - p_2) = \text{composite number}$
in contradiction to the premise that p_1 was a prime number. The assertion that $p_1 \neq 3$ can be proven analogously.

Next, it will obviously follow from the premise (b) that

$$w \equiv 2 \pmod{3} \quad (\text{C2})$$

Next we will utilize the statement (C2), Lemma C.1 to build a proof *ad absurdum*. Assume that p_1 is a lower twin different from 3. Then

$$p_2 = w - p_1 \equiv 2 - 2 \pmod{3} \equiv 0 \pmod{3}$$

But the above contradicts the premise that p_2 is prime different from 3. \square

We are finally ready to the principal theorem of this section:

Theorem C.3. *The number of even numbers possessing the NLT property is infinite*

Let us first make an estimate. According to the Prime Number Theorem, the number of primes below a number N is, approximately, $\pi(N) \approx N/\ln(N)$. It will immediately follow that for a given prime p_j , the next prime p_{j+1} will be separated from p_j by a gap—filled by the composite numbers—whose size is approximately $\ln(N)$. (Her and below, $p_1, p_2, p_3, \dots = 2, 3, 5$ is the contiguous sequence of prime numbers in ascending order.) It will also follow that $p_j \approx j \ln(j)$.

The probability that a given number N obeys the premise (b) of Lemma C.2 is $1/6$. The probability that a number of this type obeys the premise (a) is $1 - 2/\ln(N)$. Here $1/\ln(N)$ is the inverse of the gap between consecutive primes; the factor of 2 accounts for the fact that premise (b) implies that N is even and hence that $N - 3$ is odd. Now, according to the Lemma C.2, the probability that a given number N is an even number that possesses

the NLT property is $(1/6)(1 - 2/\ln(N)) \stackrel{N \gg 1}{\approx} 1/6$. All in all, we estimate that number of the even numbers obeying the NLT property that are less than N is

$$\pi_{\text{NLT}}(N) \stackrel{N \gg 1}{\approx} \frac{N}{6} . \quad (\text{C3})$$

The rigorous proof for the assertion that the number of the NLT-compliant evens is infinite will only cover a small subset of them in comparison with the ones involved in the estimate above. For that, we will identify an infinite subsequence w_k of even numbers that possess the NLT property. of the

Proof. Consider a sequence

$$\begin{aligned} w_k &\equiv 2(15k + 4) \\ k &= 1, 2, 3, 4, \dots \end{aligned}$$

Let us first show that this sequence obeys the premise (a) of the Lemma C.2. Indeed,

$$2(15k + 4) - 3 = 5(6k + 1) ;$$

the right hand side is a manifestly composite number unless $k = 0$ For the premise (b), we get

$$2(15k + 4) = 6k' + 2 ,$$

with $k' = 5k + 1$. \square

Interestingly, our subsequence properly captures the uniformity of the distribution estimated by (C3) but underestimates the density of the NLT evens:

$$\pi_{\text{NLT}}(N) \geq \frac{N}{30} - \frac{19}{15} . \quad (\text{C4})$$

-
- [1] G. Gauthier, T. A. Bell, A. B. Stilgoe, M. Baker, H. Rubinsztein-Dunlop, and T. W. Neely, Chapter one - dynamic high-resolution optical trapping of ultracold atoms (Academic Press, 2021) pp. 1–101.
- [2] T. Harte, G. D. Bruce, J. Keeling, and D. Cassetari, Conjugate gradient minimisation approach to generating holographic traps for ultracold atoms, *Opt. Express* **22**, 26548 (2014).
- [3] P. Zupancic, P. M. Preiss, R. Ma, A. Lukin, M. E. Tai, M. Rispoli, R. Islam, and M. Greiner, Ultra-precise holographic beam shaping for microscopic quantum control, *Opt. Express* **24**, 13881 (2016).
- [4] J. yoon Choi, S. Hild, J. Zeiher, P. Schauß, A. Rubio-Abadal, T. Yefsah, V. Khemani, D. A. Huse, I. Bloch, and C. Gross, Exploring the many-body localization transition in two dimensions, *Science* **352**, 1547 (2016), <https://www.science.org/doi/pdf/10.1126/science.aaf8834>.
- [5] K. Henderson, C. Ryu, C. MacCormick, and M. G. Boshier, Experimental demonstration of painting arbitrary and dynamic potentials for bose–einstein condensates, *New Journal of Physics* **11**, 043030 (2009).
- [6] G. Mussardo, The quantum mechanical potential for the prime numbers, e-print arXiv:cond-mat/9712010 (1997).
- [7] D. Schumayer and D. A. W. Hutchinson, Physics of the riemann hypothesis, *Rev. Mod. Phys.* **83**, 307 (2011).
- [8] M. Wolf, Will a physicist prove the riemann hypothesis?, *Rep. Prog. Phys.* **83**, 036001 (2020).
- [9] D. Cassetari, G. Mussardo, and A. Trombettoni, Holographic realization of the prime number quantum potential, *PNAS Nexus* **2**, pgac279 (2022), <https://academic.oup.com/pnasnexus/article-pdf/2/1/pgac279/48998652/pgac279.pdf>.
- [10] F. Gleisberg, F. D. Pumpo, G. Wolff, and W. P. Schleich, Prime factorization of arbitrary integers with a logarithmic energy spectrum, *J. Phys. B: At. Mol. Opt. Phys.* **51**, 035009 (2018).
- [11] G. Mussardo and A. Trombettoni, Integer factorization by quantum measurements, e-print arXiv:2309.10757 (2023).
- [12] F. Gleisberg, M. Volpp, and W. P. Schleich, Factorization with a logarithmic energy spectrum of a two-dimensional potential, *Physics Letters A* **379**, 2556–2560 (2015).

- [13] C. J. Foot, *Atomic Physics* (Oxford University Press, 2004).
- [14] F. Bloch and A. Siegert, Magnetic resonance for nonrotating fields, *Phys. Rev.* **57**, 522–527 (1940).
- [15] N. Khaneja, T. Reiss, C. Kehlet, T. Schulte-Herbrüggen, and S. J. Glaser, Optimal control of coupled spin dynamics: Design of NMR pulse sequences by gradient ascent algorithms, *Journal of Magnetic Resonance* **172**, 296 (2005).
- [16] J. Sørensen, J. Jensen, T. Heinzel, and J. Sherson, QEngine: A C++ library for quantum optimal control of ultracold atoms, *Computer Physics Communications* **243**, 135 (2019).
- [17] G. von Winckel and A. Borzì, Computational techniques for a quantum control problem with h1-cost, *Inverse Problems* **24**, 034007 (2008).
- [18] J. J. W. H. Sørensen, M. O. Aramburu, T. Heinzel, and J. F. Sherson, Quantum optimal control in a chopped basis: Applications in control of bose-einstein condensates, *Phys. Rev. A* **98**, 022119 (2018).
- [19] U. Dudley, *Elementary Number Theory* (W. H. Freeman and Company, San Francisco, 1969).
- [20] We exclude $0^2 + 0^2 = 0$ for technical reasons.
- [21] L. Landau and E. Lifshitz, *Mechanics: Volume 1 (Course of Theoretical Physics Series)* (Butterworth-Heinemann, Amsterdam, 1976).
- [22] S. E. Harris, Electromagnetically induced transparency with matched pulses, *Phys. Rev. Lett.* **70**, 552 (1993).
- [23] E. Arimondo, Coherent population trapping in laser spectroscopy, *Progress in Optics* **35**, 257 (1996).
- [24] Additionally, we verified that the observed drop in the cascade population is predominantly due to ionization to the continuum: the bound states outside the cascade remain unpopulated thus verifying the resonant model.
- [25] To the contrary, the sums of three squares are not closed under multiplication, e.g. $11 \times 373 = (1^2 + 1^2 + 3^2) \times (2^2 + 12^2 + 15^2) = 4103 \neq a^2 + b^2 + c^2$. Also, according to Lagrange’s four-square theorem [19] (p. 146), the set of integers that are equal to the sums of four squares coincides with the set of all natural numbers.
- [26] A relevant fact: if a is an integer that is equal to the sum of two squares, then the prime decomposition of a cannot contain a factor p^k such that p is a prime of the form $4 \times (\text{an integer}) + 3$ and k is odd.
- [27] Twin primes are a pair of primes separated by 2.
- [28] T. Caneva, T. Calarco, and S. Montangero, Chopped random-basis quantum optimization, *Phys. Rev. A* **84**, 022326 (2011).
- [29] J. J. W. H. Sørensen, M. O. Aramburu, T. Heinzel, and J. F. Sherson, Quantum optimal control in a chopped basis: Applications in control of bose-einstein condensates, *Phys. Rev. A* **98**, 022119 (2018).
- [30] C. A. Weidner, H. Yu, R. Kosloff, and D. Z. Anderson, Atom interferometry using a shaken optical lattice, *Phys. Rev. A* **95**, 043624 (2017).
- [31] C. A. Weidner and D. Z. Anderson, Experimental demonstration of shaken-lattice interferometry, *Phys. Rev. Lett.* **120**, 263201 (2018).
- [32] O. V. Marchukov and M. Olshanii, Resonance cascades and number theory, e-print arXiv:2402.04361v4 (2024).
- [33] L. D. Landau and E. Lifshitz, *Mechanics: v. 1 (Course of Theoretical Physics)* (Butterworth-Heinemann, Oxford, 2000) §12.
- [34] L. D. Landau and E. Lifshitz, *Quantum Mechanics, non-relativistic theory: v. 3 (Course of Theoretical Physics)* (Pergamon Press, Oxford, 1977) Ch. VII.
- [35] M. Olshanii, *Back-of-the-Envelope Quantum Mechanics: With Extensions to Many-Body Systems and Integrable PDEs* (World Scientific, Singapore, 2013).
- [36] N. Bleistein and R. Handelsman, *Asymptotic Expansions of Integrals* (Dover, New York, 1986).
- [37] R. Mack, J. P. Dahl, H. Moya-Cessa, W. T. Strunz, R. Walser, and W. P. Schleich, Riemann ζ function from wave-packet dynamics, *Phys. Rev. A* **82**, 032119 (2010).
- [38] M. V. Berry and K. E. Mount, Semiclassical approximations in wave mechanics, *Reports on Progress in Physics* **35**, 315 (1972).